Journal of Volcanology and Geothermal Research 188 (2009) 1–25

Contents lists available at ScienceDirect

Journal of Volcanology and Geothermal Research

journal homepage: www.elsevier.com/locate/jvolgeores

Is the track of the Yellowstone hotspot driven by a deep mantle plume? — Review of volcanism, faulting, and uplift in light of new data

Kenneth L. Pierce [a,*], Lisa A. Morgan [b]

[a] U.S. Geological Survey, Northern Rocky Mountain Science Center, 2327 University Way, Box 2, Bozeman, MT 59715, United States
[b] U.S. Geological Survey, MS 973, Box 25046, Federal Center, Denver, CO 80225, United States

ARTICLE INFO

Article history:
Received 20 August 2008
Accepted 21 July 2009
Available online 28 July 2009

Keywords:
Yellowstone
hotspot track
mantle plume
uplift
volcanism
faulting

ABSTRACT

Geophysical imaging of a tilted mantle plume extending at least 500 km beneath the Yellowstone caldera provides compelling support for a plume origin of the entire Yellowstone hotspot track back to its inception at 17 Ma with eruptions of flood basalts and rhyolite. The widespread volcanism, combined with a large volume of buoyant asthenosphere, supports a plume head as an initial phase. Estimates of the diameter of the plume head suggest it completely spanned the upper mantle and was fed from sources beneath the transition zone, We consider a mantle–plume depth to at least 1,000 km to best explain the large scale of features associated with the hotspot track. The Columbia River–Steens flood basalts form a northward-migrating succession consistent with the outward spreading of a plume head beneath the lithosphere. The northern part of the inferred plume head spread (pancaked) upward beneath Mesozoic oceanic crust to produce flood basalts, whereas basalt melt from the southern part intercepted and melted Paleozoic and older crust to produce rhyolite from 17 to 14 Ma. The plume head overlapped the craton margin as defined by strontium isotopes; westward motion of the North American plate has likely "scraped off" the head from the plume tail. Flood basalt chemistries are explained by delamination of the lithosphere where the plume head intersected this cratonic margin. Before reaching the lithosphere, the rising plume head apparently intercepted the east-dipping Juan de Fuca slab and was deflected ~250 km to the west; the plume head eventually broke through the slab, leaving an abruptly truncated slab. Westward deflection of the plume head can explain the anomalously rapid hotspot movement of 62 km/m.y. from 17 to 10 Ma, compared to the rate of ~25 km/m.y. from 10 to 2 Ma.

A plume head-to-tail transition occurred in the 14-to-10-Ma interval in the central Snake River Plain and was characterized by frequent (every 200–300 ka for about 2 m.y. from 12.7 to 10.5 Ma) "large volume (>7000 km^3)", and high temperature rhyolitic eruptions (>1000 °C) along a ~200–km-wide east–west band. The broad transition area required a heat source of comparable area. Differing characteristics of the volcanic fields here may in part be due to variations in crustal composition but also may reflect development in differing parts of an evolving plume where the older fields may reflect the eruption from several volcanic centers located above very large and extensive rhyolitic magma chamber(s) over the detached plume head while the younger fields may signal the arrival of the plume tail intercepting and melting the lithosphere and generating a more focused rhyolitic magma chamber.

The three youngest volcanic fields of the hotspot track started with large ignimbrite eruptions at 10.21, 6.62, and 2.05 Ma. They indicate hotspot migration N55° E at ~25 km/m.y. compatible in direction and velocity with the North American Plate motion. The Yellowstone Crescent of High Terrain (YCHT) flares outward *ahead* of the volcanic progression in a pattern similar to a bow-wave, and thus favors a sub-lithospheric driver. Estimates of YCHT-uplift rates are between 0.1 and 0.4 mm/yr. Drainage divides have migrated northeastward with the hotspot. The Continental Divide and a radial drainage pattern now centers on the hotspot. The largest geoid anomaly in the conterminous U.S. is also centered on Yellowstone and, consistent with uplift above a mantle plume.

Bands of late Cenozoic faulting extend south and west from Yellowstone. These bands are subdivided into belts based both on recency of offset and range-front height. Fault history within these belts suggests the following pattern: Belt I — starting activity but little accumulated offset; Belt II — peak activity with high total offset and activity younger than 14 ka; Belt III — waning activity with large offset and activity younger than 140 ka; and Belt IV — apparently dead on substantial range fronts (south side of the eastern Snake River Plain only). These belts of fault activity have migrated northeast in tandem with the adjacent hotspot volcanism. On the southern arm of the YCHT, fault activity occurs on the inner, western slope consistent with driving by gravitational

* Corresponding author. Tel.: +1 406 994 5085.
E-mail address: kpierce@usgs.gov (K.L. Pierce).

0377-0273/$ – see front matter. Published by Elsevier B.V.
doi:10.1016/j.jvolgeores.2009.07.009

potential energy, whereas faulting has not started on the eastern, outer, more compressional slope. Range fronts increase in height and steepness northeastward along the southern-fault band.
Both the belts of faulting and the YCHT are asymmetrical across the volcanic hotspot track, flaring out 1.6 times more on the south than the north side. This and the southeast tilt of the Yellowstone plume may reflect southeast flow of the upper mantle.

Published by Elsevier B.V.

1. Introduction

Along the hotspot track, many facets of the surface geology can be related to one driving process — a mantle plume. This review focuses on volcanism, faulting, and uplift associated with the track of the Yellowstone hotspot. In our earlier studies of the track of the Yellowstone hotspot (Pierce and Morgan, 1990, 1992), we examined Neogene deposits and features along a 700-km northeast-trending swath that starts with ~17 Ma volcanism near the Oregon–Idaho–Nevada border and continues northeast through a succession of volcanic fields to the 2-Ma-and-younger Yellowstone Plateau volcanic field. We suggested that the timing and location of volcanism, faulting, and uplift were related to a common mechanism: a deep-sourced mantle plume, which has been subsequently recognized by seismic tomography (Fig. 1). Building upon the results and interpretations from previous investigations (Morgan, 1972; Smith et al., 1974; Armstrong et al., 1975; Westaway, 1989; Anders et al., 1989; Malde, 1991) and our own field observations and synthesis, we presented a model for the evolution of a mantle plume and its effect upon the adjacent lithosphere over the past 17 m.y. (Pierce and Morgan, 1992). Our work and interpretations were based on the geology and structures exposed at the Earth's surface, from which we inferred what was occurring at depth. In 2002, we amplified this model mainly for the plume head area (Pierce et al., 2002), building on an accumulating body of geologic information. In our earlier studies, we showed there was a pronounced asymmetry to the hotspot track with both the bands of faulting and high terrain flaring out more to the south than to the north. We thought this might be significant, but did not offer an explanation.

Recent seismic tomography imagery has resolved a low-velocity mantle plume to a depth of 500–600 km that is inclined to the northwest from Yellowstone (Fig. 1) (Yuan and Dueker, 2005; Waite et al., 2006). Here we argue for a source deeper than that imaged based on the inferred diameter of the plume head and the breath of faulting and uplift associated with the hotspot track. For the inferred plume-head start of the hotspot track, we discuss evidence from recent seismic tomography that suggests how this plume source may have interacted with the Juan de Fuca slab. Rising of the plume westward and up the subducting Juan de Fuca slab may explain the high apparent rate of hotspot movement 17–10 Ma (62 km/m.y.). This rate is much higher than the rate of ~25 km/m.y. from 10 Ma to present, based on both the rate of Yellowstone hotspot migration and the motion of the North American plate. We relate the newly acquired seismic tomography (Fig. 1) to the surface geology along the hotspot track and discuss the evolution of the plume in terms of a three-phase model of volcanism, faulting and uplift: from 17–14 Ma, 14–10 Ma, and 10–0 Ma. The physical aspects of volcanism in each phase differ and reflect changes in plume development temporally and spatially.

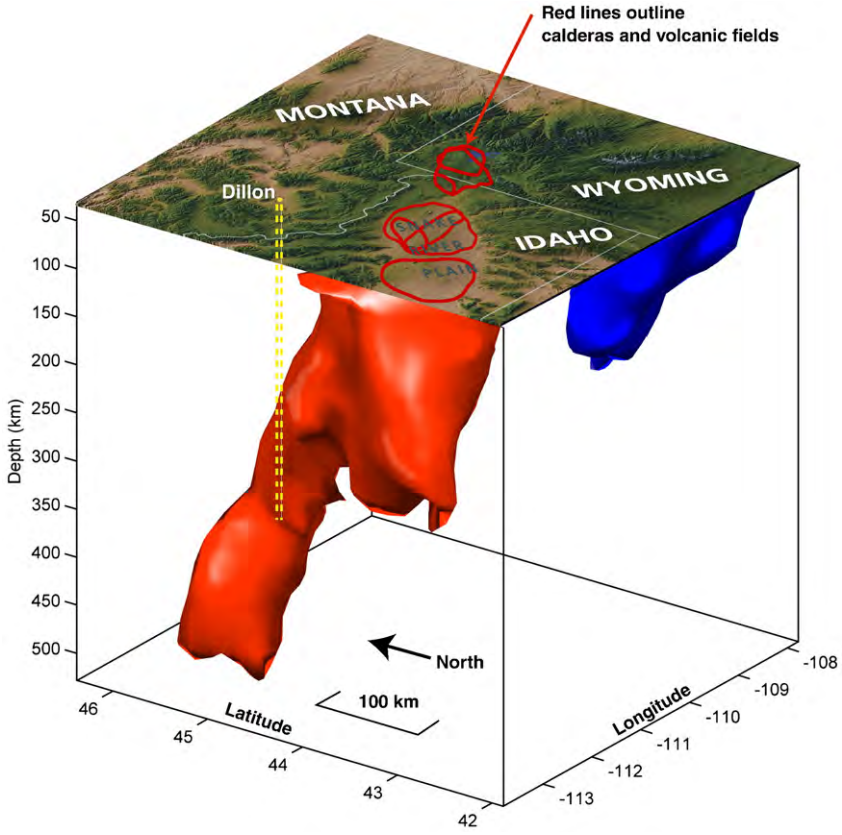

Fig. 1. Seismic tomography reveals an inclined conduit of warm mantle material (thermal plume) inclined to the northwest from beneath Yellowstone (illustration from Huaiyu Yuan, based on Yuan and Dueker, 2005). At a depth of 500 km, the inferred plume is beneath Dillon, Montana (yellow dot and dashed lines), but in this study the inferred plume was traced no deeper than 500 km. Red outlines of hotspot calderas somewhat diagrammatic and also denote the progression of volcanic fields.

Because the active (youngest) part of the Yellowstone hotspot track is now considered to be related to a thermal mantle plume (Fig. 1), it is reasonable to assume that the older part of the track that can be traced back to its inception is also the product of the same mantle plume. We also consider other factors which may have contributed to the asymmetry of the hotspot track, particularly the southeast tilt of the plume. Lastly, we consider three topics that relate to the hotspot track: (1) drainage changes; (2) helium isotopes; and (3) the depth of the inferred mantle plume.

These new plume-supporting geologic and geophysical results from the Snake River Plain–Yellowstone (SRP-Y) volcanic province are reinforced by accumulating geological, geophysical, and geochemical data on the existence of mantle plumes worldwide (for example Sleep, 1990; Davis, 1999; Ernst and Buchan, editors, 2001b; Ito and Mahoney, 2006; Montelli et al., 2006; Sleep, 2006; Campbell and Kerr (editors), 2007; Putirka, 2008).

2. Mantle plumes from Yellowstone to global

The idea of mantle plumes has been controversial since its introduction in the 1960's. Mantle plumes are an unresolved but potentially major driver of geologic processes. Morgan (1972) postulated that the SRP-Y volcanic province represented the hotspot track formed by the North American plate moving across a relatively stationary mantle plume. Armstrong et al. (1975) documented that the initiation of both rhyolitic and basaltic volcanism became younger towards Yellowstone consistent with a hotspot track. A vigorous debate has ensued as to whether or not this volcanic age progression results from a relatively fixed mantle plume beneath the southwest-moving North American plate or whether some other process can be invoked to explain the patterns observed here. Pro-plume arguments have been advanced by Suppe et al. (1975), Westaway (1989), Pierce and Morgan (1990, 1992), Draper (1991), Smith and Braile (1993), Zoback et al. (1994), Camp (1995), Parsons et al. (1994), Parsons (1995), Takahahshi et al. (1998), Thompson (1998), Rowley (2001), Pierce et al. (2002), Perkins and Nash (2002), Jordan et al. (2004), Camp and Ross (2004), Morgan and McIntosh (2005), Hooper et al. (2007), Morgan et al. (2008), Shervais and Hanan (2008), and Camp and Hanan (2008). Non-plume arguments also have been invoked for the origin of the SRP-Y volcanic province by Hamilton (1989, 2003), Smith (1992), Christiansen and Yeats (1992), Anderson (1994, 1998, 2000), Dickinson (1997, 2006), Foulger and Natland (2003); Foulger et al. (2004), Humphreys et al. (2000), Christiansen (2001), Christiansen et al. (2002), Leeman (2005), Bonnichsen et al. (2007), and many papers at http://www.mantleplumes.org.

Courtillot et al. (2003) concluded that three types of hotspots are present in the Earth's mantle: (1) those originating deep near the core–mantle boundary (at depths near 2900 km); (2) those originating from the bottom of the transition zone (at depths about 660 km); and (3) those within the upper mantle (at depths above 410 km). Conversely, modeling of outward heat dissipation and modeling whole mantle convection versus heat transfer through a layered mantle favor the likelihood of whole mantle convection over layered convection (McNamara and van Keken, 2000). Recently, estimates of the flux of heat from the core have been revised upward from 3–4 to 5–15 terawatts (Lay et al., 2008) and indicate the core is an important source for mantle heating. Although some geophysical studies image the Yellowstone plume only to the transition zone, we suggest that the basic heat source extends deeper, perhaps to the core–mantle boundary.

2.1. Mantle plume model, from head to tail

In the general mantle plume model, a plume or a thermal anomaly at higher than normal mantle temperatures is formed deep in the mantle and evolves into a two-part structure. First, a lower plume tail or conduit feeds and inflates a slowly rising plume head (Richards et al., 1989; Hill et al., 1992). As the inflating plume head (density ~3.2 g/cc) continues to rise through the upper mantle (density ~3.3 g/cc), it eventually contacts and tends to couple with the base of the lithosphere and the overriding tectonic plate. With continued plate motion carrying the plume head, the tail, fixed in the relatively stationary mantle, is detached from the plume head and itself intercepts the lithosphere where it leaves a track in the direction opposite to the movement of the overriding plate. Understanding of the details of transition from plume head to tail is murky, but apparently is recorded in the Yellowstone hotspot track in the 14–10 Ma interval.

When upwelling mantle–plume material rises to within 100–200 km of the Earth's surface, decompression melting produces a basaltic magma (density ~3.0 g/cc, ~10% melt) that provides the magma or the heat for extensive flood basalt eruptions over a large area (diameter >500 km). Basalt magma from decompression melting may also transfer heat to lighter, silicic crust, producing rhyolitic magma (density ~2.7 g/cc). For both the plume head and tail, decompression melting of the rising mantle (density ~3.25 g/cc) yields both a basaltic melt plus a remaining residuum (restite) that have lower densities (~3.0 g/cc) than the original mantle. Thus, both products are more buoyant than the original mantle and may cause regional uplift (Jordan, 1979; Morgan et al., 1995).

3. Review and discussion of the Yellowstone hotspot track

The continuity of the Yellowstone hotspot track from its present position at Yellowstone back in time to its association with extensive middle Miocene volcanism in Nevada, Oregon, and Washington conforms to the plume head/tail model proposed by Richards et al. (1989). We and others (Pierce and Morgan, 1992; Perkins et al., 1998; Link et al., 1999; Hughes and McCurry, 2002; Perkins and Nash, 2002) envision the thermal plume at Yellowstone evolving over three phases.

3.1. Phase I (17–14 Ma): inception of the Yellowstone hotspot: influences of the plume head on geology

Approximately 17 Ma, an ascending spheroidal plume head with an estimated diameter of 300 km (see Section 3.1.3) is inferred to have intercepted the base of the lithosphere, flattening outward into a disk with a diameter of ~1000 km at the base of the North American plate. This plume head has been invoked to explain (Fig. 2): (1) the outburst of flood basalt volcanism to the north in Washington and Oregon; (2) the intrusions forming a large basaltic dike system in northern and central Nevada to the south; and (3) the rhyolitic volcanism in northern Nevada and adjacent Oregon and Idaho (Pierce and Morgan, 1990, 1992; Draper, 1991; Parsons et al., 1994; Camp, 1995; Parsons, 1995; Takahahshi et al., 1998; Thompson, 1998; John et al., 2000; Glen and Ponce, 2002; Pierce et al., 2002; Camp and Ross, 2004; Jordan et al., 2004) and southern Nevada (Rowley, 2001). In addition, Geist and Richards (1993) suggest a rising plume intercepted the obliquely north-moving Farallon slab and enlarged while being carried north to beneath the geometric center of Columbia River flood basalts.

3.1.1. Volcanism

The track of the Yellowstone hotspot starts with a large area of 16.7-to-14-Ma flood basalt and rhyolite volcanism that extends hundreds of kilometers outward from its nominal center near the Nevada–Oregon–Idaho border (Fig. 2). About 95% of the estimated volume of 234,000 km^3 of Columbia River and Steens flood basalts (CR-SB) was erupted within a 2-m.y. interval (Baksi, 1989; Tolan et al., 1989; Carlson and Hart, 1988). More recently, Camp and Ross (2004) concluded the flood-basalt phase lasted only 1.5 m.y. Two discoveries extend the plume-head volcanism further southwest. (1) The ~15.4-Ma, 150-km^3 Lovejoy basalt correlates temporally with CR-SB-flood

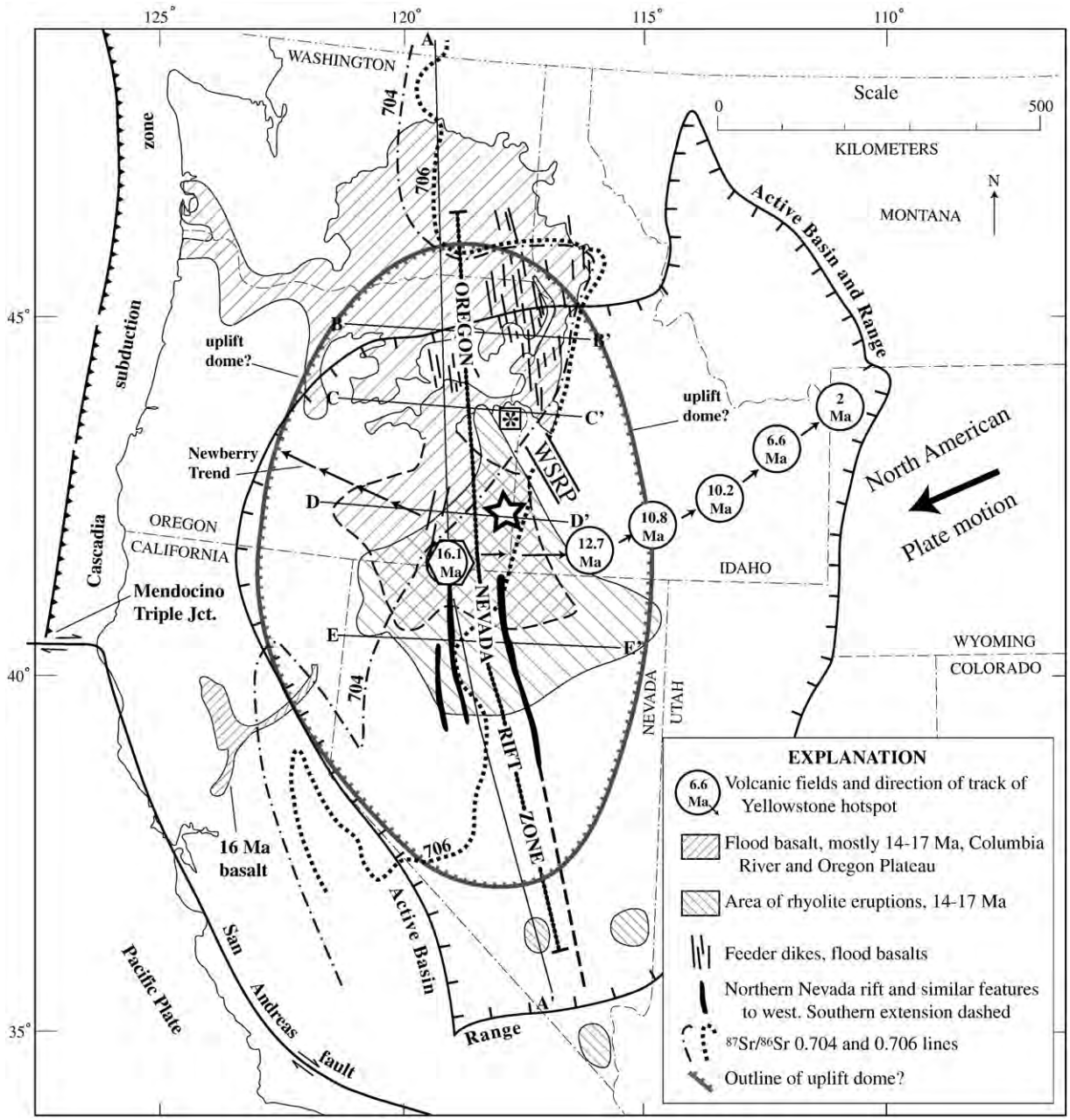

Fig. 2. Map of western United States showing the track of the Yellowstone hotspot (after Pierce and Morgan, 1992). Extent of 17–14-Ma flood basalts, dikes, and rhyolites indicates a process we consider driven by the Yellowstone mantle plume head. The Northern Nevada rift zone (wide black masses) is extended (dashed line) by magnetic anomalies to southern Nevada. We consider three options for the starting -plume center (from south to north):1) Hexagon — backtracking of the rhyolitic hotspot track to start near 16.1 Ma McDermitt caldera (Pierce and Morgan, 1992), 2) Star — focus of dike swarms after correcting for block rotation (preferred location) (Ernst and Buchan, 2001a,b) and 3) Square with * — convergence of present dike and fold trends (Glenn and Ponce, 2002). Hachured gray line delimits uplift dome (?) from Pierce et al. (2002). North–south transect A–A′ is portrayed in Fig. 3. BB′, CC′, DD′, and EE′ are latitudinal bands for age relationships between volcanism, dike intrusion and extension by faulting (Fig. 7). 16 Ma flood basalt in California from Wagner et al. (2000). Extending of Basin and Range into northwestern Montana after Lageson and Stickney (2000).

basalts and erupted in northeast California, flowed 240 km southwest, ponded to considerable depth in the northern Great Valley, and almost reached San Francisco (Fig. 2) (Wagner et al., 2000; Garrison et al., 2008); and (2) Coble and Mahood (2008) recognize four 16.5–15.5-Ma caldera-forming, silicic fields in northwestern-most Nevada that they attribute to the start of the Yellowstone hotspot.

The vast majority of CR-SB flood basalts were emplaced through thin, dense, Mesozoic oceanic crust, whereas to the south 14–17-Ma rhyolites, dispersed about the inferred hotspot center, were generated in thicker, less dense and more silicic crust (Fig. 3) (Draper, 1991; Pierce and Morgan, 1992; Pierce et al., 2002; Camp and Ross, 2004; Hooper et al., 2007). For the rhyolites, Shervais and Hanan (2008) suggest their generation was aided by delamination at the front of the plume head. The contrast of basalt versus rhyolite generally follows the silicic versus mafic crustal compositions that are delineated by the initial $^{87}Sr/^{86}Sr$ 0.706 and particularly the 0.704 contours (Fig. 2).

Many recent petrologic studies of the CR-SB flood basalts support a mantle plume origin. Hooper et al. (2007) conclude that a mantle plume model has several merits: (1) the earliest Columbia River basalt flows "…contain the chemical and isotopic signatures of ocean island basalts" and have high $^{3}He/^{4}He$ ratios, both considered indicators of a deep mantle source; and (2) flood basalts are noted to occur at the

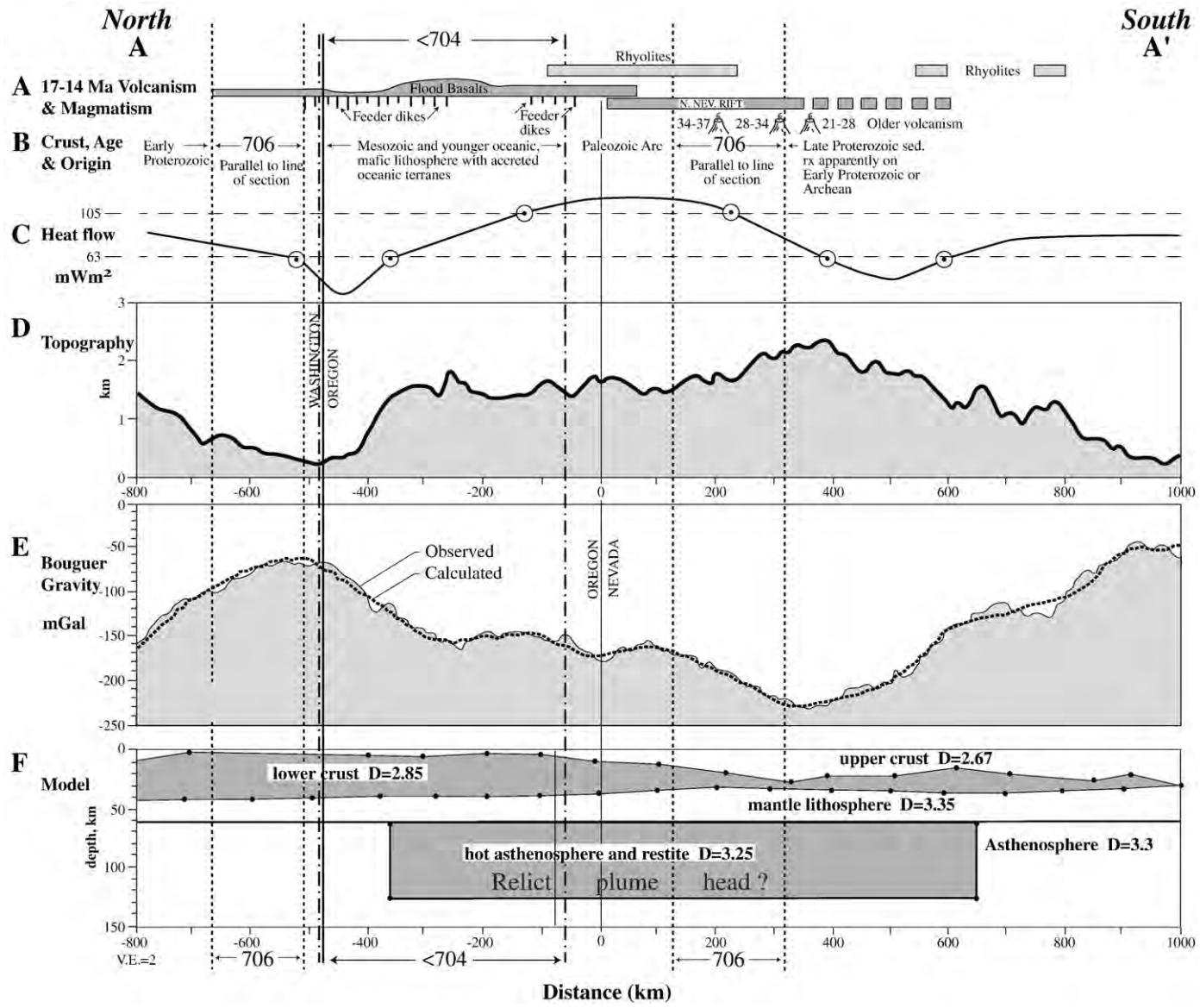

Fig. 3. North–south section (A–A′ Fig. 2) showing geologic features relevant to plume head hypothesis (after Pierce et al., 2002). The strontium isotopic boundaries ($^{87}Sr/^{86}Sr$) define crustal boundaries such that continent-ward of the 706 line is Precambrian silicic continental crust; ocean-ward of the 704 line is Mesozoic and younger mafic oceanic crust. A. 17–14 Ma magmatism. Rhyolite eruptions overlap both the southern part of the flood basalts and the mafic, rift-filling dikes of the Northern Nevada rift. The 14–17-Ma rhyolites fade out roughly in the area where older magmatism (21–37-Ma) had already occurred and the crust thus became more refractory. B. Crust ages and origin. Precambrian designations from Link et al. (1993). Northern Nevada divisions from Elison et al. (1990). Oregon crust from Draper (1991) showing 2–4 km volcanic and volcaniclastic rock over 15–20 km of oceanic crustal material; Carlson and Hart (1987) show this as new crust over depleted upper mantle. C. Heat flow (in mW m^{-2}) from Morgan and Gosnold (1989). More recent heat flow data is shown at Blackwell's SMU heat flow site: http://www.smu.edu/geothermal/heatflow/heatflow.htm. D. Regional topography (average of five profiles spaced 15 km apart centered on section A–A′). E. Regional complete Bouguer gravity anomaly (same profiles as in D). The data are from the Decade of North American Geology (DNAG) data compilation for the conterminous United States (Hittelman et al., 1994). Dashed line shows fit to model shown below in F. F. Gravity model of lithosphere and upper asthenosphere. The large low density anomaly in the upper mantle (shaded) may be a relict plume head. Crust/mantle boundary taken from an average of several Moho maps (Mooney and Weaver, 1989; Pakiser, 1989; Braile et al., 1989). The boundary between the upper (felsic) and lower (mafic) crust was allowed to vary between sea level and the Moho (base of lower crust) to match the Bouguer anomalies. This model shows that the gravity data are consistent with a crust that is largely mafic to the north and felsic to the south.

initial stages of plume-related volcanism. In the SRP-Y province, flood basalts occur in the earliest and western end of the Yellowstone hotspot track and are followed over the next ~16 m.y. by an eastward march of rhyolitic volcanism to the Yellowstone Plateau volcanic field, beneath which a mantle plume is identified. This hotspot track of rhyolite supports the concept that rhyolite can be produced by a mantle plume acting beneath cratonic crust, and this may also be the genesis of ~17–15-Ma rhyolite in the plume head area. We infer this progression to be continuous and prompted by the same source—a mantle plume that has evolved over time. Hooper et al. (2007) also note that the greatest volume of flood-basalt volcanism occurred in the areas of least extension and conclude that "extension alone, no matter how advanced, can not generate the melt volumes typical of continental flood basalt provinces."

Hales et al. (2005) conclude that a dense lithospheric root beneath the Wallowa Mountains in northeast Oregon (Chief Joseph dike swarm) detached and thereby made space for upward rising mantle material, which then caused greater decompression melting and subsequent eruption of Imnaha and Grande Ronde flood basalts. For northeastern Oregon, Hales et al. (2005) explain a high velocity mantle as buoyant mantle residuum left after decompression melting. This interpretation for the Grande Ronde Basalt explains why basaltic melts whose heat is derived from thermal plumes may have chemistry more related to the mantle lithosphere than occurs with simple

decompression melting of a mantle plume. With a differing interpretation of chemical isotopic sources, Wolff et al. (2008) use mixing-trend diagrams to argue that the Grande Ronde basalts in northeast Oregon include a component from the craton farther to the south–southeast.

3.1.2. Lateral plume flow, plume-triggered delamination, and flood basalts

As defined by the initial $^{87}Sr/^{86}Sr$ 0.704 and 0.706 lines (Fig. 2), the lithosphere might be expected to thin from the older Precambrian craton in the east to the younger Mesozoic accreted terranes both to the west and north from the inferred plume center position (Fig. 2 star; Fig. 4). As shown in Fig. 4, spreading of the plume head beneath this cratonic-to-oceanic boundary may have increased melt formation in two ways. First, the inferred thinner oceanic Mesozoic lithosphere to the northwest may have accentuated flow to higher levels and enhanced decompression melting in "thinspots" (Thompson and Gibson, 1991; Sleep, 1997). Second, this discontinuity may provide a site for delamination and sinking (drip) of mantle lithosphere, thus vacating space for further rise and decompression melting of plume material, plus additional melts derived from lithospheric masses sinking into the hot mantle plume (Camp and Hanan, 2008; Burov et al., 2007; Hales et al., 2005).

Camp and Hanan (2008) explain the complex sequence of changing chemistry, location, and extrusion rate for the CR-SB flood basalts as a result of northward-spreading plume head and associated delamination created by Rayleigh–Taylor instabilities (denser material above lighter material). They adapt (their Fig. 8) numerical models of Burov et al. (2007) for a plume head beneath 150-Ma lithosphere that spreads northward over a distance of 300 km to abut against a thick Precambrian cratonic boundary near the Washington–Oregon border. These numerical models are consistent with progressive generation of basaltic melts as the plume head spread rapidly to the north. In chronological order, the sequence can be divided into four parts:

(1) Initially, from near the center of the plume head in southeast Oregon, delamination of mantle lithosphere "drips down" into the hot plume head and is melted to produce the Steens flood basalts;

(2) A mass of mantle lithosphere starts to delaminate allowing a wedge of plume-head material to ascend to the base of the crust so that enhanced decompression melting yields and erupts plume-type Imnaha basalt;

(3) Some mantle lithosphere with attached mafic lower crust further detaches and sinks into the hot plume head where the attached mafic lower crust rapidly melts to produce the huge outpouring of aphyric Grande Ronde basaltic andesite. This satisfies the suggested origin of the Grande Ronde basaltic andesite as melts of mafic pyroxenitic or eclogitic source from mantle depths (see Wright et al., 1989; Takahahshi et al., 1998; Hooper et al., 2007, and Camp and Hanan, 2008);

(4) The plume head pushes northward against the edge (keel) of Archean (or Paleoproterozoic) craton, resulting in the eruption of the Wanapum and Saddle Mountain basalts that are a mix of melt from plume basalt and Archean lithosphere.

The topography, stress regime, and lithospheric structure of southeast Oregon to southeast Washington are similar to those used in the numerical models of Burov et al. (2007) for plume-head delamination (Camp and Hanan, 2008, their Fig. 8).

3.1.3. Upper mantle density deficiency

A N–S section (Fig. 2, AA′) transects the Basin and Range and shows geologic parameters relevant to the plume-head hypothesis as follows (Fig. 3, parts A–F): (A) flood basalts to the north and rhyolitic deposits and mafic–rift intrusions to the south; (B) Mesozoic mafic lithosphere to the north grades southward to Precambrian crust; (C) heat flow values are elevated across a large area where the plume head is inferred to have first intercepted the base of the lithosphere; (D) a broad topographic high centers in northern Nevada; (E) a broad Bouguer gravity anomaly low is centered in northern Nevada; and (F) a density model of the crust and upper mantle (Fig. 3F) closely fits the observed Bouguer gravity shown in part E and has a large, buoyant plume-like mass in the asthenosphere. Higher gravity values on the northern half of the inferred plume head are accounted for by denser mafic lower crust consistent with younger mafic oceanic lithosphere. This 2-D model (Fig. 3F) is similar to the 3-D model of Parsons et al.

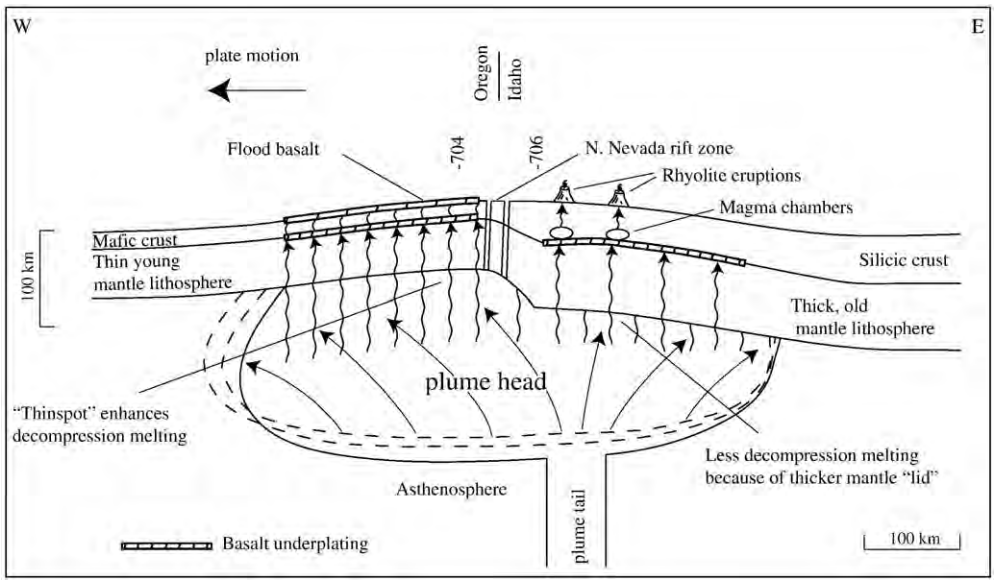

Fig. 4. Diagrammatic west–east cross section near common boundaries of Oregon, Idaho, and Nevada showing effect of lithospheric contrast on flow in the plume head and on "shearing off" of the plume head. Old silicic craton above thick mantle lithosphere is east of initial $^{87}Sr/^{86}Sr$ 0.706 isopleth and young mafic accretionary crust with thinner lithospheric mantle is west of initial $^{87}Sr/^{86}Sr$ 0.704. The buoyant plume head flows upwards towards the "thinspot" where upwelling to shallower depths enhances decompression melting and thereby provides more melt for flood basalts. Just east of the axis of flood basalt volcanism, extension of the Oregon–Idaho graben was between 15.3 and 12.6 Ma (Cummings et al., 2000) and of the western Snake River Plain between 11 and 9 Ma (Wood and Clemens, 2002). This extension is younger than the main phase of flood basalt volcanism and thus mantle upwelling due to this extension was not responsible for the flood basalts. As the North American plate moves southwest (left), the plume head shears off from the plume tail, and stays with the plate, trapped by the inferred deeper keel of the older, thicker lithosphere to the east.

(1994) which indicated a mantle mass deficit (~3.6×10^{18} kg) exists beneath most of the northern Basin and Range. Parsons et al. (1994) conclude that "such a mass deficit is comparable to the expected deficit (~$3–8.5\times10^{18}$ kg) from a small plume head ~400-km radius (Hill et al., 1992) that is 100–300 °C hotter than the surrounding asthenosphere." We suggest the low density asthenosphere in Fig. 3F ($D=3.25$ g/cc) represents a flattened plume head. It is 1000-km-long by 65-km-deep for a cross-sectional area of ~65,000 km^2; this has the equivalent area as a circle with a diameter of 288 km, here rounded to 300 km. Because the section A–A′ (Fig. 2) of Fig. 3 was selected to go through the center of the plume head, the diameter of the spherical plume head is estimated to be about 300 km. This is considerably smaller than the plume head modeled by Parsons et al. (1994) with a diameter of 800 km; thus our 300-km-diameter plume head may be a minimum estimate.

3.1.4. Plume head fed from below the upper mantle?

Although geophysical studies by Yuan and Dueker (2005) and Waite et al. (2006) conclude the current Yellowstone plume extends to only ~500 km depth in the mantle transition zone, we suggest that a plume extends deeper based on the size of the starting plume head. As noted above, the mass deficit in the plume head volume (Fig. 3F) is modeled by a plume head with a diameter of 300 km. The 1000-km north–south span of tectonic and volcanic effects attributed to the plume head support a flattened disk of an original sphere of at least such a diameter. Fig. 5 shows that a 300-km-diameter plume head would completely fill the upper mantle and that any plume tail feeding this head but extending no deeper than 500 km seems too small to be potent enough to inflate and sustain the plume head (Pierce et al., 2007). If one accepts the 800-km-diameter plume dimensions of Parsons et al. (1994), this size plume head would have extended several hundred km below the base of the lithosphere and well into the lower mantle.

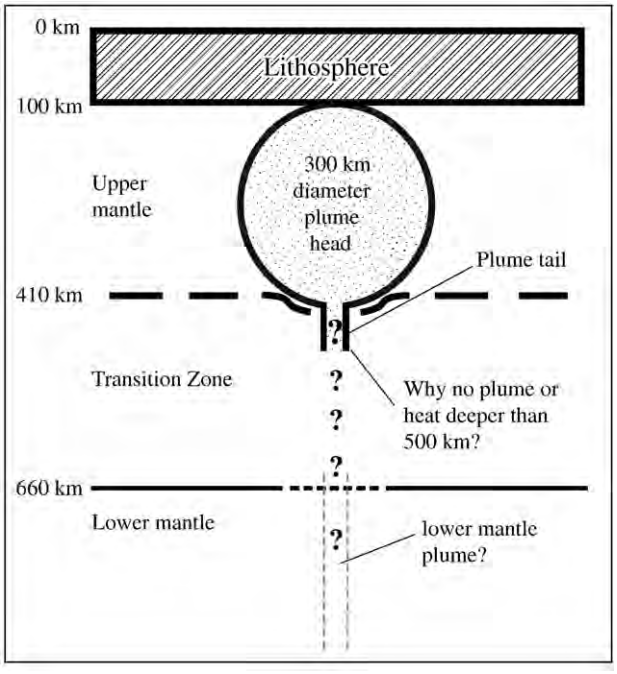

Fig. 5. Diagram showing that 300-km diameter plume head occupies the entire upper mantle (lithosphere to transition zone) at the 17-Ma start of the hotspot track. If, as suggested by imaging of the present mantle plume, the plume extends no deeper than ~500 km, then at the start of the hotspot track, the size of the plume head permits little room for a heat source and plume tail to feed the plume head. The dashed vertical lines represent a hypothetical plume in the lower mantle that may have fed the plume head. Richard Allen (see text) has imaged such a plume extending to at least 1000 km beneath the upper mantle Yellowstone plume (Fig. 1).

3.1.5. Westward offset of rising plume head by subducting Juan de Fuca slab

About 20 Ma, a rising Yellowstone plume is inferred to have encountered, penetrated, and broken the east-dipping Juan de Fuca slab (Geist and Richards 1993; Pierce et al., 2002, their Fig. 3). Xue and Allen (2007) use this mechanism to explain the abrupt termination of the Juan de Fuca slab identified now at a depth of 400 km (Fig. 6). This predicted

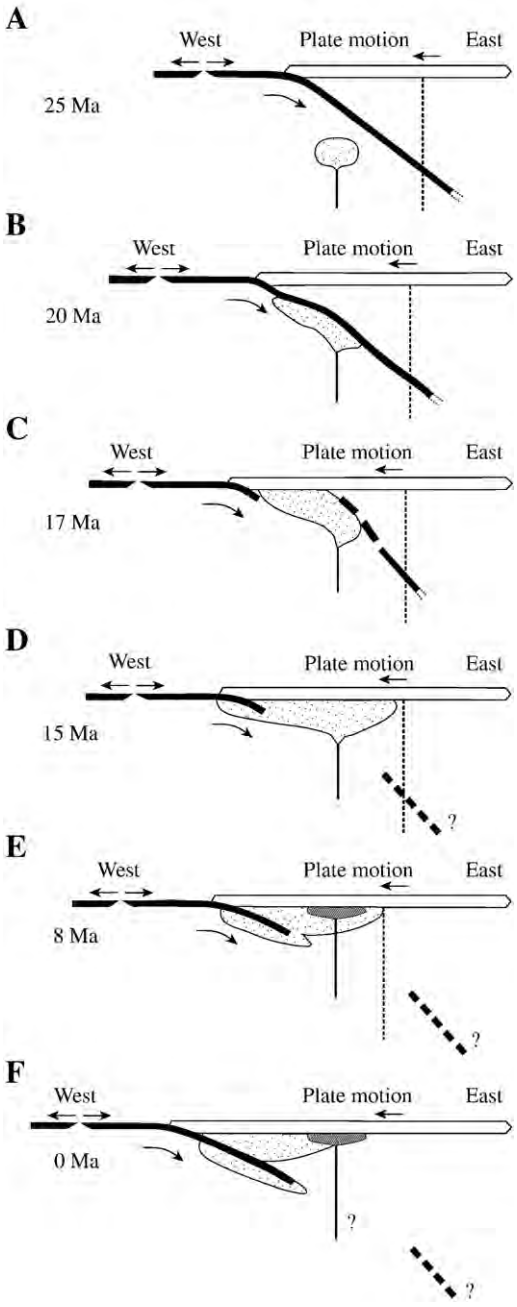

Fig. 6. Model for interaction between subducting Juan de Fuca plate and slab (thick black) and the Yellowstone plume head (stippled) and tail (thin black and dark cross hatched) (after Xue and Allen, 2007). At 25 Ma, the plume head is below the slab. At ~20 Ma the head has intercepted the slab and is diverted westward, up beneath the slab. At ~17 Ma, the head has penetrated and fragmented the slab, and by 16-Ma flood basalts are surfacing through the North American plate (open thick plate). By 15 Ma, the plume has trimmed the slab westward to its intersection with the North American plate and some of the plume's head spreads to beneath the slab. At 8 Ma, the newly subducted slab has sunken deeper in the upper mantle, and a layer of warm material (indicated by geophysics) is trapped beneath the slab. At present (0 Ma), the new slab has sunken to a depth of 400 km, but has a sharp lower end clearly shown in the geophysics and that is explained as broken off by the plume head at 17 Ma. Vertical dotted line is reference position of Yellowstone in North American plate.

slab encounter also would produce the apparent westward offset of the plume head that is needed to explain the unreasonably high rate of hotspot migration and inferred North American plate motion of 62 km/m.y., about 2.5 times faster than both the 10–2 Ma hotspot migration rate (~25 km/m.y.) and the North American Plate rate of a~25 km/m.y. (Gripp and Gordon, 2002). Conversely, Roth et al. (2008) find that only a small section of the Juan de Fuca slab has detached. They also consider that the apparent "hole" in the slab is an inversion artifact produced by the presence of low velocity material above the slab. Changes in mantle flow (mantle winds) might also explain this anomaly.

3.1.6. Debate on where the plume head intercepted the lithosphere

Several locations have been advocated for the center of the plume head as follows (Fig. 2):

(1) The hotspot track of silicic volcanism starts with the initial caldera-forming rhyolite eruption at 16.1 Ma in the McDermitt volcanic field and therefore has been considered to be the nominal plume center (Malde, 1991; Pierce and Morgan, 1990, 1992; Zoback et al., 1994; Parsons et al., 1994; Pierce et al., 2002).

(2) Geist and Richards (1993) suggest a plume, but not a plume head, was trapped and accumulated beneath the Farallon slab eventually resulting in its breakthrough and continued ascent beneath the common borders of Idaho, Washington, and Oregon (see Fig. 2) where the Grande Ronde, Imnaha, and Wanapum flood basalts were erupted. However, a problem with this location for the plume-head center is that it is in the northern, younger, rather than southern, older sequence of outwardly radiating flood basalt eruptions documented by paleomagnetic polarity reversals (Camp and Ross, 2004).

(3) Based on radiating dikes in an area along the Oregon–Idaho border (Fig. 2, * symbol in square), an alternative center was mapped by Glen and Ponce (2002) at a convergence of dikes and folds. Shervais and Hanan (2008) advocate this position based on the plume head originally centering in this location but crowded by the craton to the east as well as deflected towards thinner extended lithosphere to the SE.

(4) Also using radiating mafic dikes but correcting for block rotations using paleomagnetic data, Ernst and Buchan (2001a) placed the plume head center about 80 km north of the Nevada–Oregon border (Fig. 2, star). Basaltic dikes here are more directly related to the plume head rather than the somewhat later silicic volcanism at McDermitt (16.1-Ma volcanic field on Fig. 2). It also is in the center of the outward pulse of dike injection based on a sequence of magnetic polarity changes (Camp and Ross, 2004, their Fig. 6) and the location we favor.

3.1.7. Uplift associated with the plume head

Hotspots are commonly accompanied by large topographic swells 1–2 km high and a thousand or more km across (Fig. 2, gray oval line showing postulated uplift dome after Pierce et al., 2002) (Crough, 1978; Şengör, 2001). The plume-head model predicts that uplift will start before the actual contact of the plume with the lithosphere (Hill et al., 1992). Although uplift is a difficult process to geologically quantify, thirteen lines of evidence consistent with plume-head uplift are summarized in Pierce et al. (2002). For northwest Nevada, Coble and Mahood (2008) invoke mid-Miocene uplift to explain major canyons cut by overtopping of caldera lakes at 16.5–15.5 Ma.

Closely related to density deficits is the relatively high altitude of the inferred plume head area, both now and more significantly at the time of the start of the hotspot track. The observed Basin-and-Range extension after 16 Ma and the resultant crustal thinning would result in subsidence. Paleobotanical studies indicate that at ~15 Ma central Nevada was about 1–1.5 km higher than at present (Wolfe et al., 1997). The Columbia River flood basalts show a sequence of progressively more northern basalt eruptions that record a northward expansion of doming interpreted to result from progressive northward spreading of the plume-head accompanying CR-SB volcanism (Camp, 1995; Camp and Ross, 2004; Hooper et al., 2007).

Stable isotope studies of authigenic calcite and smectite also indicate surface lowering of the central Basin and Range province since middle Miocene time (Horton and Chamberlain, 2006). In northern Nevada, similar stable isotope studies show uplift during the Oligocene followed by subsidence after the middle Miocene (Horton et al., 2004). The Oligocene uplift is ~>10 m.y. before plume head impact and earlier than the pre-volcanism uplift interval modeled by Hill et al. (1992) suggesting that modification of the plume-head model or additional mechanisms need to be pursued to explain this uplift.

Recent studies by Wallace et al. (2008) suggest that northeastern Nevada was an upland in middle Tertiary time until ~16 Ma and that following this period, the region's main westerly drainage, the Humbolt River, captured areas further east across the inferred axis of the plume-head dome. About 50 km east of the Northern Nevada Rift, which is assumed to be on the axis of plume head uplift (Fig. 2), the inferred plume crest was actually crossed by a drainage from the east (Wallace et al., 2008). At ~16 Ma, drainages in northeastern Nevada were impounded as a result of volcanic damming or possible tectonic changes (Wallace et al., 2008). Shortly after 16 Ma, faulting offset both paleohighlands and basin sediments. Later, the west-flowing Humbolt River extended farther westward across the inferred center of the plume head terrain which Wallace et al. (2008) suggests may be associated with subsidence of the plume head area.

3.1.8. Relationship between volcanism and extension

Age relationships between volcanic activity, normal faulting, and dike injection for the past 20 Ma are depicted (Fig. 7) for four east–west bands (Fig. 2). CR-SB volcanism preceded graben formation (Taubeneck, 1970; Hooper, 1990; Hooper et al., 2007). First, extension follows rather than precedes volcanism and extension actually increases from north to south whereas volcanism increases from south to north. Both this timing and north–south diminution of volcanism are inconsistent with extension causing volcanism (Hooper, 1990; Hooper et al., 2007). From north to south the zones in Fig. 7 show:

BB′ — Eruption of the voluminous Grande Ronde flood basalt occurred after the start of smaller-volume flood basalt volcanism to the south (see DD″) (Hooper et al., 2007; Camp and Ross, 2004). Dike intrusion that represents only minor extension (<l%; Hooper, 1990) was accompanied, most notably, by the Chief Joseph dike swarm.

CC′ — Eruption of the Picture Gorge basalts occurred shortly after the start of the Grande Ronde flood basalt eruptions (Camp and Ross, 2004). Flood basalt volcanism occurred first, followed by extension to form the Oregon–Idaho Rift (west of WSRP in Fig. 2) (Cummings et al., 2000) and the western Snake River Plain (see Fig. 2) (Wood and Clemens, 2002).

DD′ — The earliest flood basalt volcanism was initiated with eruption of the Steens Basalt, which was immediately followed by normal faulting to the west (Hooper et al., 2007).

EE′ — Mafic dikes were injected into the Northern Nevada Rift Zone (Zoback and Thompson, 1978) with only moderate basalt extrusion. Following the start of flood basalt volcanism, eruptions of rhyolite were widespread and may indicate that basalt underplating was widespread as well. Normal faulting in north-central Nevada was significant ~12–10 Ma and even greater ~6–5 Ma (Wallace et al., 2008). In northwest Nevada, faulting was significant 10–7 Ma (Colgan et al., 2004; see part 3.1.9.).

Thus, as well argued by Hooper (1990), the mid-Miocene record does not show large extension before CR-SB volcanism (Fig. 7) and hence does not support the idea of decompression melting of mantle material moving upward into extension-created space as a precursor to flood basalt volcanism. The assumption that back-arc-spreading drove CR-SB flood volcanism (Carlson and Hart, 1988; Smith, 1992) does not fit the timing in that volcanism precedes extension. Instead,

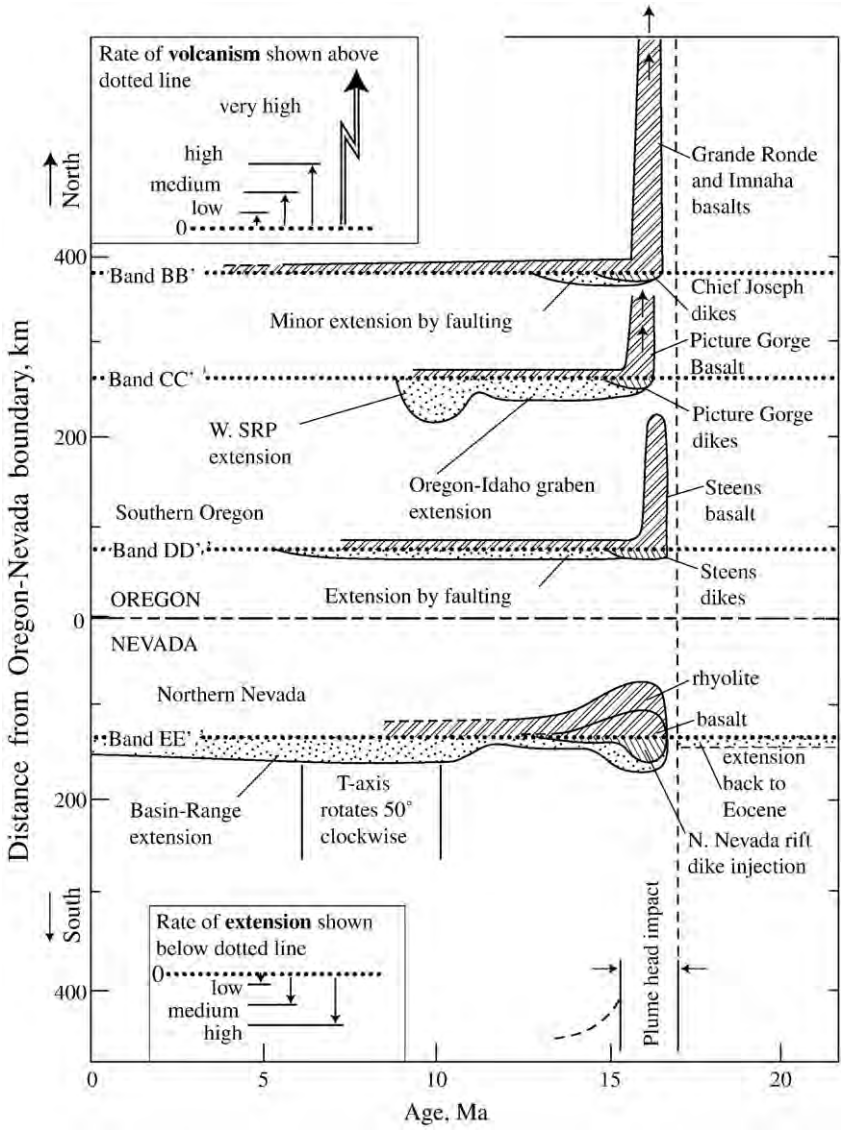

Fig. 7. Cartoon comparing relative rates of volcanism, faulting, and dike injection over the last 20 Ma at four different latitudes across the inferred plume area (indicated by bands BB′, CC′, DD′, and EE′; see Fig. 2). The thicknesses of the fill patterns above or below the dotted lines indicate the relative rates of three processes: (1) volcanism (above the dotted line, double-line cross-hatch); (2) extension by normal faulting (below the dotted line, stippled); and (3) extension by dike injection (below the dotted line, single cross hatch). The scale for relative rate of volcanism is in upper left, and scale for extension is in lower left. As shown by diagrams, volcanism precedes rather than follows significant extension. Thus, mantle upwelling driven by crustal extension, as for example in back arc spreading (Smith, 1992), does not precede and thereby does not drive CR-SB flood basalt volcanism. For bands BB′, CC′, and DD′, this figure is a graphical illustration of the relation noted by others that flood basalt volcanism preceded extension, including Hooper (1990), Camp (1995), and Hooper et al. (2007). For band EE′, references are Colgan et al. (2004, 2006, 2008); Wallace (2005), Zoback and Thompson, (1978), Zoback et al., (1994). The relative rates of volcanism in Bands CC′ and DD′ are both very high, but that in Band BB′ is highest.

evidence supports flood basalt volcanism occurring first, followed in places by extension millions of years later (Fig. 7). Rather than significant mantle upwelling driven by little or no extension, an additional process that we infer to be a mantle plume is needed (Hooper, 1990; Camp and Ross, 2004; Hooper et al., 2007).

3.1.9. Relationship of the plume head to Basin and Range extension

Numerous geologic events are associated with the inception of the Yellowstone hotspot track particularly in the northern Basin and Range province (Fig. 2). Given the 700-km-long Yellowstone hotspot track (Fig. 2) and the recent discovery of a deep plume beneath the 0.64-Ma Yellowstone caldera, it is logical to infer that the plume at Yellowstone is the same one responsible for previous volcanism along the hotspot track, and that this plume is the descendant of a plume head responsible for the start of the hotspot track. As just described, the initial location for the plume head is now inferred to be north of the center of the Basin and Range (Fig. 2) and has a strong temporal (~17 Ma) tie but somewhat off-center spatial tie to the mid-Miocene main phase of Basin and Range extension (Parsons, 1995; Dickinson, 2006; Fosdick and Colgan, 2008).

Extension of the Basin and Range has been attributed to multiple causes (see Dickinson and Snyder, 1979; Atwater, 1989; Severinghaus and Atwater, 1990; Parsons, 1995; Dickinson, 1997; Dickinson, 2006) including (1) back-arc extension between 50 Ma and 30 Ma, a time frame clearly preceding inferred plume-head activity at 17 Ma; (2) extensional spreading following orogenic over-thickening in Laramide–Sevier time; (3) divergence between the North American plate and the Pacific plate; (4) a slab window permitting warm asthenospheric mantle to reach the base of the lithosphere and produce volcanism and softening of the crust; and (5) uplift and thermal softening associated with the Yellowstone plume head (Pierce and Morgan, 1992; Pierce et al., 2002).

The role of the Yellowstone hotspot in Basin and Range extension, particularly during the plume head phase, may involve: (1) uplift providing a gravitational potential; and (2) heating and weakening of

the lithosphere and asthenosphere facilitating westward movement. Uplift is difficult to quantify but appears to have occurred (Fig. 2, gray oval) (Pierce et al., 2002; Camp and Ross, 2004; Beranek et al., 2006). Perhaps the most persuasive evidence, a kind of "still smoking gun", is the buoyancy anomaly in the upper mantle attributed to the stagnant Yellowstone plume head (Parsons et al., 1994; Parsons, 1995; Saltus and Thompson, 1995; Pierce et al., 2002). The above factors support a relationship between Basin-and-Range extension and the postulated plume head. Other factors, however, also are involved for Basin-and-Range extension that extend much farther south into Mexico "well out of reach of even a large [Yellowstone] plume head" (Parsons, 1995).

Gravity-driven westward extension and associated faulting of the lithosphere may have started on the west side of the inferred plume head uplift (Hill et al., 1992; Camp and Ross, 2004) and continues now in the northern Basin and Range province. In the area of the Northern Nevada Rift, extension rotated about 45° from S68°W at 16 Ma to N65°W at present (Zoback and Thompson, 1978).

The plume-head hypothesis may apply to the relative altitude decrease from the northern to the southern Basin and Range (Saltus and Thompson, 1995). The western boundary of the North American plate is weakly confined by the Pacific and Juan de Fuca plates (Humphreys and Coblentz, 2007; Bohannon and Parsons, 1995), thereby providing an "escape" for extension to the west in the northern Basin and Range. If so, the northern Basin and Range might be regarded as a large, low-gradient lithospheric landslide that extends down from the Yellowstone Crescent of High Terrain westward to the weakly confined western boundary of the North American plate at the Cascadia subduction zone. Another recent observation documenting northwest extension of the Basin and Range comes from GPS motions relative to the North American reference frame (Kreemer and Hammond, 2007). They isolate a "window of escape" in northern California from latitude ~38° to 42° north where reduction of area (compression) equals aerial increase in the Basin and Range (extension).

For northwestern Nevada, the total amount of extension is about ~12% and began about 11–12 Ma (Colgan et al., 2006). For northern Nevada just west of the Northern Nevada rift (Fig. 2), extension began at or shortly after 16 Ma and was mostly completed by 10–12 Ma (Colgan et al., 2008). In the Windermere Hills of northeastern Nevada, a fundamental change in extension occurred following Oligocene low-angle faulting. Starting at ~15 Ma and continuing to 7 ± 2 Ma or younger, closer spaced normal faults that formed grabens are considered by Mueller et al. (1999) to result from "extensional stresses imparted to the base of the lithosphere by a laterally spreading mantle plume (e.g., the Yellowstone hotspot) located in southeastern Oregon at this time." Thus, a major phase of Basin Range extension started ~15 Ma shortly after volcanism attributed to the plume head and continued for at least several million years.

3.1.10. Mineralization related to the plume head

Extensive epithermal gold–silver mineralization in northern Nevada 15.0–15.6 Ma is temporally and spatially related to the Northern Nevada Rift and the plume head phase of the Yellowstone hotspot (John et al., 2000; John and Wallace, 2000; John, 2001; Kamenov et al., 2007). Mafic magmas associated with the Yellowstone hotspot carried gold up into epithermal systems "where precious metals precipitated together with quartz and adularia to form bonanza ores that typify these deposits" (Kamenov et al., 2007). John (2001, his Fig. 9) diagrammed the bimodal basalt–rhyolite assemblage and associated mineralization that began ~16.5 Ma as derived from a basaltic "mantle plume" melt.

3.1.11. The Yellowstone plume head and the Newberry volcanic trend

The progression of rhyolitic eruptions northwestward across southern Oregon from ~11 Ma in the southeast to <1 Ma at Newberry to the northwest has been used to argue against the Yellowstone track as a mantle plume (Christiansen and Yeats, 1992; Lipman, 1992; Christiansen et al., 2002). The west–northwest Newberry trend (Fig. 2) intersects the start of the Yellowstone hotspot track at an angle ~120° counterclockwise from the Yellowstone hotspot trend. The Newberry track becomes defined at 11 Ma and the rate of west–northwest advance of volcanism slows towards the Newberry end. Compared to the large-volume ignimbrites of the Yellowstone hotspot track, the Newberry trend consists mostly of local rhyolite domes and small-volume ignimbrites, with the exception of the extensive Rattlesnake Tuff (MacLeod et al., 1976; Christiansen and Yeats, 1992; Pierce and Morgan, 1992; Pierce et al., 2002; Streck and Grunder, 2008). In their study of the Newberry trend, Jordan et al. (2004) addressed problems with four models and favored spreading of a plume head westward from thick to thin lithosphere aided by subduction-induced counterflow. Conversely, using shear wave splitting to determine olivine orientation, Xue and Allen (2006) find mantle shear orientation does not fit counterflow and conclude the rhyolite progression is the product of lithosphere-controlled processes. In summary, the origin of the Newberry Trend is uncertain, but its rhyolite age progression is not a sufficient argument to negate the Yellowstone hotspot as a mantle plume.

3.2. Phase II: the transition: plume head to plume tail (~14–10 Ma)

Between the inferred plume head to plume tail phases of the hotspot track, we and others (Pierce and Morgan, 1992; Morgan et al., 1997; Perkins et al., 1998; Perkins and Nash, 2002; Hughes and McCurry, 2002; Bonnichsen et al., 2007; Shervais and Hanan, 2008) infer a transitional phase. Phase II is based on the distribution and timing of igneous events between the plume head phase (Phase I, 17 to 14 Ma) and the plume tail phase (Phase III, 10.2 Ma to present). Phase I involves the ballooning head of the thermal plume slowly rising through the mantle (Fig. 6) and intercepting and spreading out at the base of the lithosphere. In Phase II, we and Shervais and Hanan (2008) suggest that the bulk of the plume head remained west of a major lithospheric boundary where it was banked against the thicker, more cratonic lithosphere that occurs east of the $^{87/86}$Sr 0,706 line (Figs. 2 and 4). As the North American plate continued to move to the southwest, the plume head was likely "sheared off" from the plume tail that fed the head (Fig. 4). The 14-Ma-and-younger eruptions appear to represent the early part of this transition, and the east–west band of eruptions from 13 to 7.5 Ma (Fig. 8, after Bonnichsen et al., 2007) represents the main part of this transition. Based on abundant volcanic ash layers in Miocene sediments, Perkins and Nash (2002) documented a large number of Yellowstone-track rhyolitic eruptions between 10 and 12 Ma, referring to this as the "rhyolite flare up." Based on the estimated location of two calderas which erupted around 10.2 Ma but were 200 km apart, Morgan et al. (1997) suggested that the transition area covered over a >200-km-long section of the hotspot track and suggested the heat source was spread over that distance and over a time interval lasting until ~4 Ma. As shown by Bonnichsen et al. (2007), volcanism in the transition occurred over a 7-m.y. interval (Fig. 8). Only the volcanic field inception ages of 12.5 and 10.8 Ma show a systematic northeast "hotspot" migration (Fig. 2). Bonnichsen et al. (2007) attribute this non-systematic swath of extensive volcanism shown in Fig. 8 to upwelling related to extension and are uncommitted regarding a mantle–plume explanation. We suggest that volcanism and extension was driven by a combination of the thinner eastern margin of the plume head and the penetration by of the plume tail to the base of the lithosphere. In addition, extension and development of the western Snake River Plain graben was concentrated in this same Phase II area (Fig. 2); extension was apparently prolonged here because the Idaho batholith to the east resisted extension (Pierce and Morgan, 1992).

The apparent early rate of hotspot movement from McDermitt (16.1 Ma) to the Twin Falls field (10.8) was ~62 km/m.y. This is more

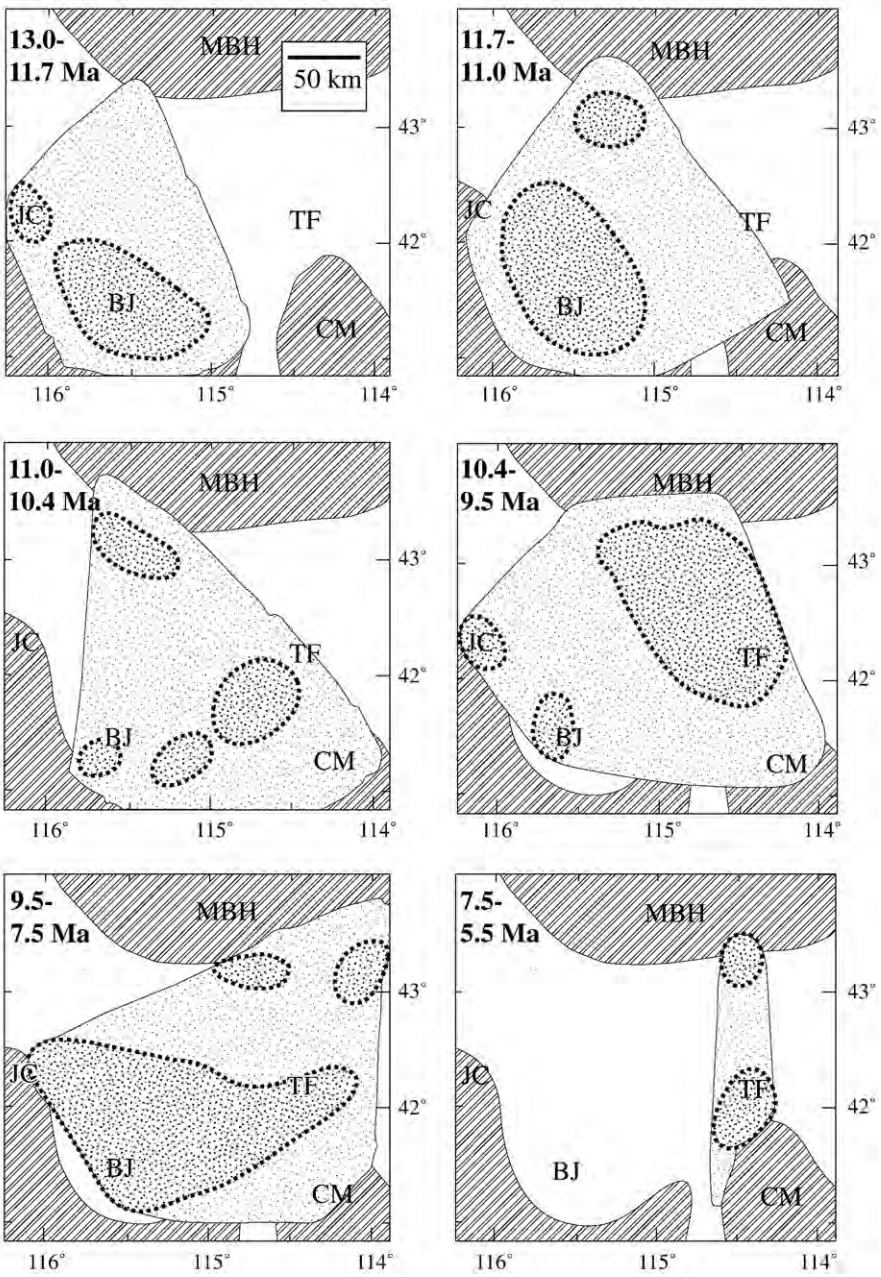

Fig. 8. Extent and sources of rhyolite eruptions in the central Snake River Plain (CSRP) at six time intervals (from Bonnichsen et al., 2007). For locations on Fig. 1, the Bruneau Jarbridge field (BJ) is field that started 12.5 Ma, and the Twin Falls (TF) is the field we conclude started 10.8 Ma. The intervals of volcanic activity are given in million years. The areas within the dotted lines indicate volcanic sources active in the given time interval. Stippled areas indicate the general extent of ignimbrites and rhyolites lavas for the time interval. Diagonal hachured areas are highlands bordering the CSRP: CM — Cassia Mountains, MBH — Mount Bennett Hills. JC — Jack Creek volcanic center. Although the onset of volcanism has a tendency to migrate easterly, the activity in the CSRP through time is dispersed and non-linear, particularly when compared to the Eastern SRP.

than twice as fast as both: (1) the maximum ~25 km/m.y. hotspot track rate (extension subtracted from the initial Picabo caldera eruption at 10.2 Ma to the initial Yellowstone caldera at 2.05 Ma) (Fig. 9); and (2) the North American plate rate of about 27 km/m.y. (Gripp and Gordon, 2002). Geist and Richards (1993) suggested the elevated rate of hotspot movement was from the plume snapping to an upright position after its release from the Juan de Fuca slab. As discussed earlier (Section 3.1.5), the fitting the plume-head model to the paleo-plate-tectonic configuration at 16 Ma, the plume head may have been deflected ~260 km westward as it rode up the underside of the east-dipping Juan de Fuca (or Vancouver slab; Pierce et al., 2002). A recent geophysical study concludes that the Juan de Fuca slab was penetrated and fragmented by the Yellowstone plume head in such a fashion (Fig. 6) (Xue and Allen, 2007, p. 273). Another study did not find a major break in the Juan de Fuca slab (Roth et al., 2008).

The Owyhee–Humbolt volcanic center is east of the nominal plume center at McDermitt and near the tri-state boundaries of Oregon, Nevada, and Idaho. It includes 17–15-Ma basalt and 16–13.8-Ma rhyolite (Bonnichsen and Kaufman, 1987; Bonnichsen and Godchaux, 2002). Although we once showed this as a discrete volcanic field (Pierce and Morgan, 1992), we and others do not now consider it readily distinguishable from the 14 to 17 Ma plume-head volcanism. In the northern part of the Owyhee–Humbolt area, the Juniper Mountain center erupted rhyolites between 14.5 and 13.5 Ma (Manley and McIntosh, 2002). The Juniper Mountain center might be regarded as the earliest part of the Phase II transition.

In contrast to the widely dispersed 17–14-Ma Phase I volcanism, Phase II volcanism changed in character as the hotspot progressed eastward from the Bruneau–Jarbridge volcanic field (inception age 12.7 Ma) through the Twin Falls volcanic field (10.8 Ma) to the Picabo volcanic field (10.2 Ma). The Bruneau–Jarbidge field had frequent eruptions and high eruptive temperatures (>1000 °C) whereas the

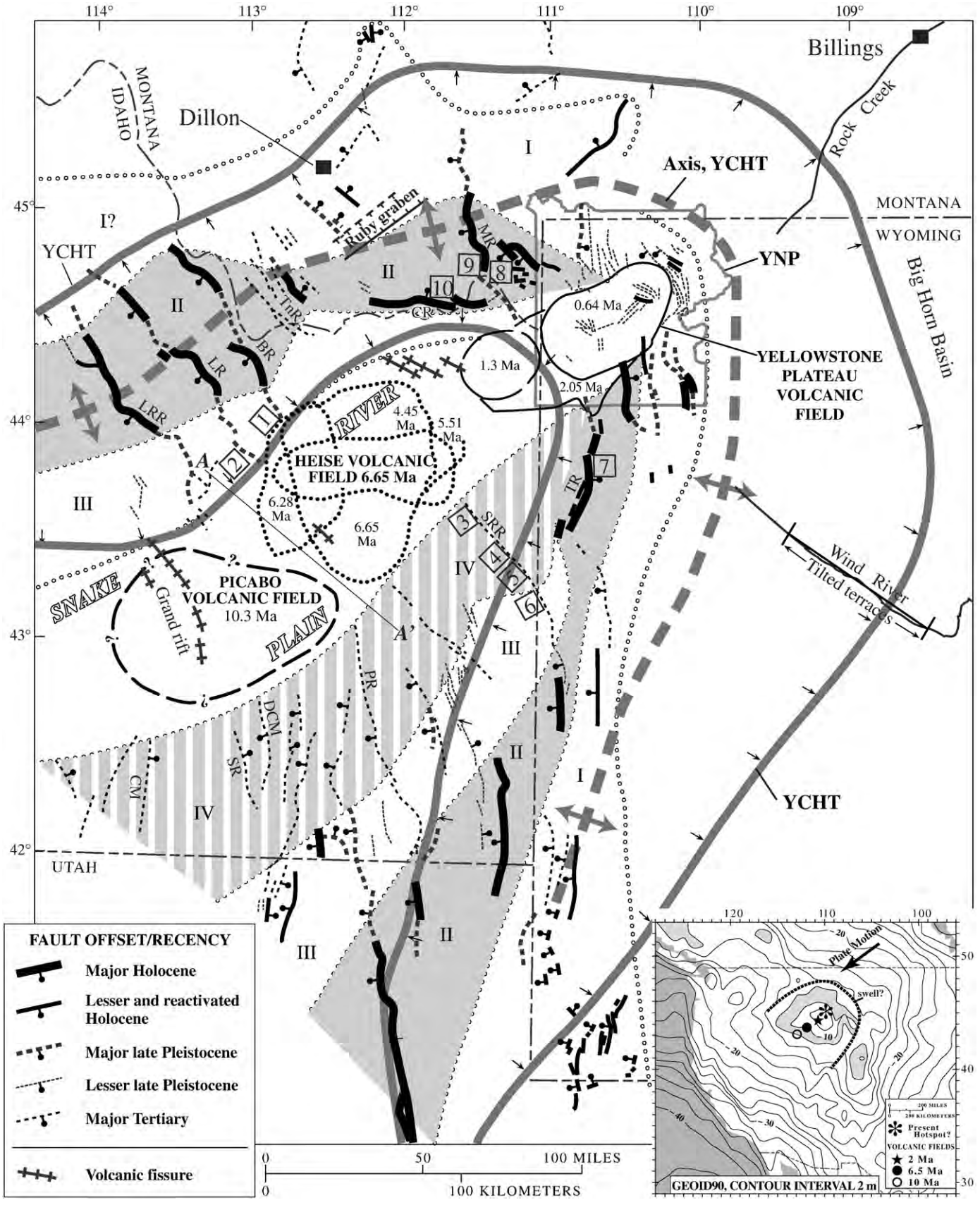

Picabo field had fewer large-volume eruptions and lower eruptive temperatures (700–850 °C). Hughes and McCurry (2002, their Fig. 8) diagram a model that extends down into the upper mantle and shows: (1) thinner Paleozoic crust with magmas ponding at temperatures between 950 and 1050 °C at greater depth for the Twin Falls field (10.8 Ma, Fig. 2); and (2) to the east, thicker Precambrian crustal depths with ponding at shallower depths of cooler (850–950 °C) magmas for the later Picabo field. Phase II volcanism is more confined than Phase I but affects a northeast-trending area about 200–300 km in length and about 90–100 km wide in the central Snake River Plain. Here, volcanism was frequent (every 200–300 ka from ~12.7 to 10.5 Ma, voluminous (Bonnichsen et al., 2007) and progressed eastward but also continued in the west and was widespread throughout the transition area. This pattern suggests possibly the following: (1) that the broad transition area required a heat source of comparable area; and (2) the differing characteristics of the volcanic fields (Bruneau–Jarbidge, Twin Falls and Picabo) may be attributed to differing crustal compositions but also may be due to developing over differing parts of an evolving plume: the older Bruneau–Jarbidge and Twin Falls volcanic fields may reflect the eruption of several large volcanic centers located above a very large extended rhyolitic magma chamber(s) over the detached plume head while the Picabo volcanic field may signal the arrival of the plume tail now separated from the plume head and intercepting and melting the base of the lithosphere and generating a somewhat smaller, although still large, rhyolitic magma chamber. Volcanism in this new plume tail phase affects a more focused area (100 km^2).

3.3. Phase III, 10 Ma (Picabo) to present (Yellowstone) activity

3.3.1. The 10-Ma-and-younger interval of the hotspot track is defined by a progression of three volcanic fields with inception ages as follows (Figs. 1 and 9): Picabo (10.21 Ma), Heise (6.62 Ma), and Yellowstone Plateau (2.05 Ma)

Flaring outward from this volcanic track in a bow-wave fashion are south- and west-trending bands of faulting and the YCHT. The geophysical confirmation of a mantle plume, discussed next, confirms our previous conclusion that, based on the surface geology, the best explanation of the hotspot track is a mantle plume.

3.3.2. Geophysical discovery of a mantle plume

Two tomographic studies reveal evidence that a plume with slower seismic velocities considered to represent warmer mantle material rises up to the southeast and encounters the lithosphere beneath Yellowstone (Fig. 1) (Yuan and Dueker, 2005; Waite et al., 2006). These studies concluded that this plume-like feature extends no deeper than ~500 km which is in the mantle transition zone (between ~660 km and ~410 km). Recently Smith et al. (2007, 2009-this volume) extend this low-velocity body to 650 km. A deeper continuation of the Yellowstone plume has been imaged from the transition zone to a depth of at least 1000 km using finite frequency tomographic analysis (Allen et al., 2008; Richard Allen *in* Lay, 2009). This analysis used a larger array larger than previous tomographic studies, one that extends to the west coast of the United States.

A thermal plume rising through the mantle transition zone is thought to result in a thinner transition zone as a result of mineralogical phase changes. Thus, the ~410-km discontinuity at the top of the transition zone (see Fig. 5 for transition zone) is predicted to be somewhat deeper and the ~660-km discontinuity at the base of the zone to be shallower. In fact, the Yellowstone plume does deepen the ~410-km discontinuity; however, no clear deflection of the ~660-km discontinuity is observed (Fee and Dueker, 2004). As discussed later (Section 3.6.3), "phase changes" may be associated with a "hot" 660-km discontinuity and obscure the expected upward deflection.

Geophysical transects across the eastern Snake River Plain 230 km southwest of Yellowstone across the 6–10-Ma section of the hotspot track (Fig. 9, Section A–A′) reveal several features. Here upward deflection of the 660-km discontinuity (thinning of the transition zone) is interpreted to indicate hotter material; however, upward deflection of the 410-km discontinuity (not the expected downward deflection and thinning of the transition zone) suggests cooler material (Humphreys et al., 2000). Beneath the hotspot track of the Snake River Plain, the asthenosphere is inferred to be hot to a depth of almost 200 km with as much as 2% melt in a zone about 170 km across (Humphreys et al., 2000). Further analysis of low-velocity material beneath the hotspot track up to 300 km southwest of Yellowstone reveals an extremely low S-wave velocity zone (3.8 ± 0.1 km/s) at a depth of 80 km and excess temperatures of >55°–80 ° C (Schutt et al., 2008; Schutt and Dueker, 2008) that may represent a sheared off plume-tail layer. Although Christiansen et al. (2002) have argued that the <1 Ma rhyolitic and basaltic magmatism in the same area is inconsistent with the mantle–plume hypothesis, we suggest this hot material in the ~10-to-6-Ma part of the hotspot track is readily explained by plate-motion shearing, as well as by outwelling of mantle plume-tail material.

Outside the still-hot mantle along the track and extending out to more than 350 km beneath both sides of the Plain is high velocity mantle. This material is considered by Humphreys et al. (2000) to be mantle residuum left over after 5–10% basalt was extracted by decompression melting of rising mantle material. Compared to normal asthenosphere, this residuum is less dense but has higher velocity (Jordan, 1979) and would contribute buoyancy to the Yellowstone crescent of high terrain (YCHT).

3.3.3. Volcanism

Along the hotspot track, the first large-volume ignimbrites for the most recent three volcanic fields define a linear hotspot track (Fig. 9) (Pierce and Morgan, 1992). Inception ages are 10.21 Ma for the Picabo volcanic field, 6.62 Ma for the Heise volcanic field, and 2.05 Ma for the Yellowstone Plateau volcanic field. This track is well expressed by the 90 to 100-km-wide topographic trench of the eastern Snake River Plain. The driving force for this youngest part (phase III) of the hotspot track is well explained by the plume tail concept of Richards et al. (1989).

The progression of phase III volcanic fields advances N 55° E at 29 km/m.y. over the last 10 m.y. as determined from their locations and inception ages (Pierce and Morgan, 1992, not corrected for extension). The HS3-NUVELI North American plate motion rate at Yellowstone predicts a volcanic track vector of N 69.5° E ± 10.7° at 26.8 ± 7.8 km/m.y. (Gripp and Gordon, 2002). Rodgers et al. (2002, their Fig. 3 and Fig. 19 caption) calculated an extension factor on the south side of the ESRP of 1.21. They corrected our 29 km/m.y. rate for Basin-and-Range extension and note "… that the difference between Pierce and Morgan's migration rate ($29 \text{ km} \pm 5$/m.y.) and the Basin and Range rate extension rate (4–6 km/m.y) is equivalent to independently calculated North American plate migration rate of 22 ± 8 km/m.y. (Gripp and Gordon, 1990), evidence in support of a hotspot origin of the eastern SRP."

3.3.4. Faulting

One band of active faults extends southward from Yellowstone and another extends westward from Yellowstone, forming a bow

Fig. 9. Yellowstone hotspot track for past 10 Ma showing volcanism, faulting and Yellowstone Crescent of High Terrain (YCHT). Fault classification shown in lower left. Faults with >500 m range-front relief are classified as Major. Fault belts are interpreted as follows: Belt I — incipient activity (or rejuvenation); Belt II — culmination of activity, Belt III — waning of activity, and Belt IV — inactivity. Inset in lower right shows Yellowstone geoid anomaly. Numbers in squares show location of faults with high-activity intervals as plotted Fig. 10. Ranges and bounding faults (north of ESRP): MR — Madison Range, CR — Centennial range, TnR — Tendoy Range, BR — Beaverhead Range, LR — Lemhi Range LRR — Lost River Range. (South of ESRP): TR — Teton Range, SRR — Snake River Range and Grand Valley fault, PR — Pocatello Range, DCM — Deep Creek Mountains, SR — Sublette Range, CM — Cotterel Mountains. A more detailed color map showing topography is available at: http://nrmsc.usgs.gov/staff/kpierce.

wave-like pattern flaring out from the hotspot volcanic track (Anders et al., 1989; Pierce and Morgan, 1990, 1992; Smith and Braile, 1993). Pierce and Morgan (1992) subdivided these bands into four belts of neotectonic activity based on recency of offset and range-front height (Fig. 9). On the outer leading edge is Belt I that is characterized by faults with post-glacial (<14 ka) offsets but low or insignificant range-front heights, or, on the north side of the ESRP, reactivated faults. Inside Belt I is Belt II that contains major Holocene faults on range fronts >700 m high. Inside Belt II is Belt III that is characterized by major late Pleistocene (<130 ka) faults on range fronts >500 m high. Finally inside Belt III, but only on the south side of the track, is Belt IV that is characterized by deactivated late Tertiary or older Quaternary faults on range fronts >300 m high. (color map available at http://nrmsc.usgs.gov/staff/kpierce/pubs).

There is a strong correlation between the belts of faulting and seismicity. Seismicity flares outward about the hotspot track and is concentrated between an inner and outer parabola (Anders et al., 1989; Smith and Braile, 1993). In detail, gaps in the historic seismicity occur where there are active Quaternary faults. For example, there was a gap in seismicity along the Lost River fault prior to the surface ruptures produced by the 1983 Borah Peak earthquake, and currently, the major Holocene Teton fault is seismically quiet.

Through time, faulting has migrated in a parabolic pattern (bow wave-like) northeastward with volcanism (Anders et al., 1989; Pierce and Morgan, 1992). As shown in Fig. 10, Anders (1994) determined the intervals of high activity for 12 faults and showed that such high activity intervals migrated northeastward in a parabolic pattern at a rate of 22 km/m.y. with the stretching by extensional faulting subtracted out. This rate correlates well with the extension-corrected volcanic migration rate of about 25–23 km/m.y. from 10.2 Ma to 2 Ma (Rodgers et al., 2002) and the North American plate rate of 26.8 ± 7.8 km/m.y. (Gripp and Gordon, 2002, HS3-NUVEL1, calculated value). Such a northeastern march of activity is consistent with the interpretation that the four belts of fault activity are a progressive sequence migrating in tandem to the northeast in a bow wave-like pattern. In summary (Fig. 9), Belt I is new or reactivated faults (waxing), Belt II is the culmination of activity, Belt III is decreasing (waning) activity, and Belt IV (south side of the track only) is near cessation of activity (dead) (Pierce and Morgan, 1992).

Fig. 11 diagrammatically shows the relationship between active faulting and the inner slope of the YCHT, particularly for the southern belt where extension is nearly perpendicular to the trend of fault belts. The crest of the YCHT represents a "hump" across which the North American plate is moving to the southwest. On the western slope of this hump, potential gravitational energy is available to drive extension by normal faulting. In contrast, on the eastern slope of this hump, faulting is absent or minor, consistent with compression (or non-extension) as the North American plate moves southwest up and over this hump.

On the south side of the eastern Snake River Plain (ESRP), the range fronts become higher and steeper eastward, changing in tandem with age of nearby hotspot track volcanism and recency of faulting (Fig. 12). The young, active Teton fault, located adjacent to the present hotspot, has a very high steep range front escarpment. From there westward, the range fronts become less high and steep to the southwest. This pattern is, in part, a function of increasingly older intervals of faulting and greater time for the ranges to erode, the range front slopes to degrade, and the adjacent basins to fill with sediment. For instance, the Teton fault has been active mainly from 4.5 Ma to present (Pierce and Good, 1992; Morgan et al., 2008). In contrast, the Portneuf fault was highly active about 9–6.5 Ma. The main episode of basin-fill sedimentation associated with the Portneuf fault occurred between 9 and 7.5 Ma (Rodgers et al., 2002, their Fig. 9) whereas along a northern strand of the Portneuf fault zone rapid offset is dated between 7 and 6.5 Ma (Kellogg and Lanphere, 1988, p. 15). The age of volcanism along the track of the hotspot also gets older to the southwest. Fig. 12 shows clearly the geomorphic muting of range fronts as the age of faulting gets older to the southwest. This trend is likely combined with other factors. For example, the Teton Range front (Fig. 12) is formed of resistant Precambrian rocks whereas range fronts to the west (Fig. 12, #2–5) involve more erodible sedimentary rocks of the Sevier thrust belt.

Trenching studies of the Lost River and Lemhi faults (north of the SRP, Fig. 9) reveal that along the southern parts of both faults, two or

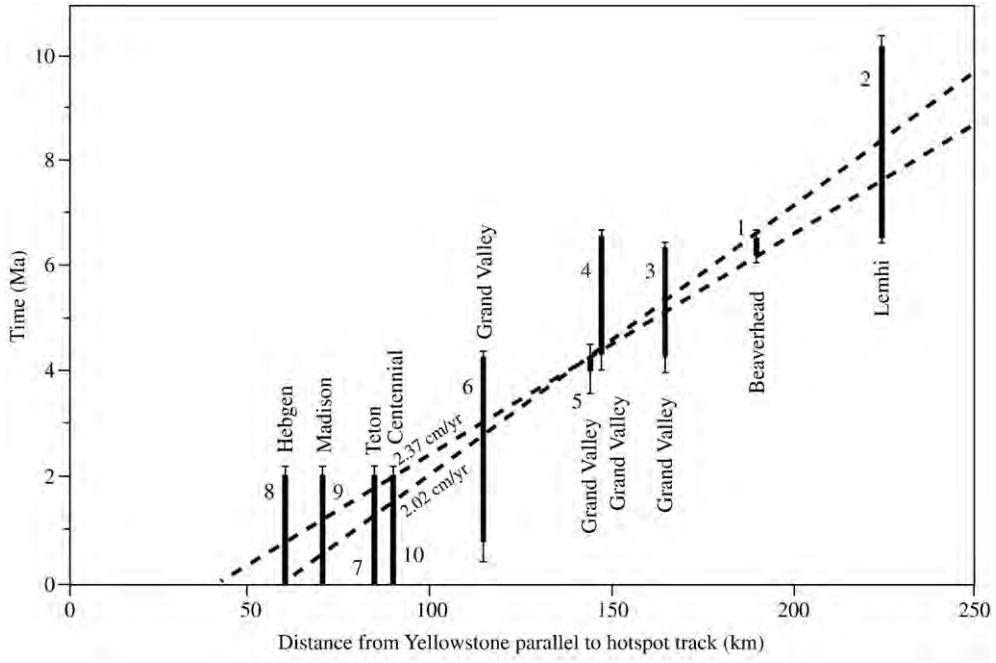

Fig. 10. Migration of intervals of high fault activity adjacent to hotspot track towards Yellowstone (after Anders, 1994). Locations of numbered faults are shown in Fig. 9. Distance is measured by translation parallel to the hotspot track from the vertex of the parabola of modern seismic activity (Anders et al., 1989). The determined rate of migration of high fault activity is between 2.02 and 2.37 km/m.y., very similar to the North American plate velocity as well as the rate of advance of large caldera-forming volcanism from 10 to 2 Ma. Although there may be debate about the precision of dating the intervals of high fault activity, such as with the Teton fault, the overall progression of activity associated with the hotspot migration is clear.

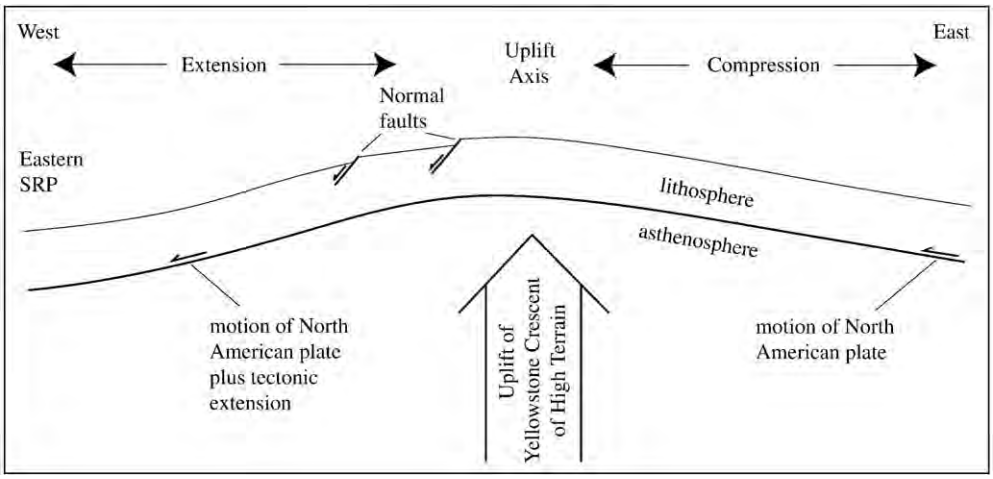

Fig. 11. Diagram of gravity driven extensional faulting down inner slope of the Yellowstone Crescent of High Terrain (YCHT). Section across the southern limb of the YCHT where fault belts I, II, and III are on the inner, western slope of the YCHT (Fig. 9). On the eastern slope (right side of figure) movement of the North American plate over the hump would foster compression and limit extension. This figure is a more localized expression of the gravitational potential energy and westward spreading that Humphreys and Coblentz (2007) attribute to the Yellowstone hotspot geoid anomaly.

more offsets are clustered in the 18–25-ka range (Olig et al., 1995, 1997; Hemphill-Haley et al., 2000). Whereas the recognition of the young timing of these offsets does not change the map designation as "major Late Pleistocene" and the boundaries of Belt III (Fig. 9), it does, however, indicate that a cluster of two events occurred not long before 15 ka. Possibly these events were associated with an interval of basaltic rift activity near-by, such as on the Great Rift on the ESRP (Fig. 9, GR).

At the base of the inner slope of the YCHT is the ESRP. Quaternary basalts erupted along rifts that trend at high angles to the margins of the ESRP and the hotspot track (Fig. 9) (Kuntz et al., 1992). Fissures on the ESRP change strike so as to be parallel to normal faults that strike northerly on the south side of the ESRP and northwesterly on the north side. These fissures are at a high angle to the hotspot track and ESRP (Fig. 9) (Kuntz et al., 1992; Pierce and Morgan, 1992; Parsons et al., 1998; Waite and Smith, 2002; Janecke et al., 2001). Such fissures record extension parallel to the axis of the hotspot track and are at nearly right angles to orientations expected if the ESRP were, as argued by Hamilton (2003), a northeast-trending rift zone.

The cumulative extension recorded by Basin and Range faulting adjacent to the ESRP is 15–21% (Rodgers et al., 1990, 2002). Rodgers et al. (2002) divide the timing of tectonism adjacent to the ESRP into three phases: (1) minor extension beginning 16–11 Ma; (2) regional subsidence and major extension starting 11–9 Ma and then migrating northeast to Yellowstone and occurring slightly northeast of coeval silicic magmatism; and (3) ongoing regional subsidence that continued southwest of coeval silicic magmatism. Subsidence based on the plunge of Cretaceous fold hinges toward the ESRP defines a zone of flexure 20 km wide that accommodated 4.5–8.5 km of subsidence into the ESRP (McQuarrie and Rodgers, 1998; Rodgers et al., 2002). On the inactive south side of the ESRP, late Cenozoic basin fill is incised by the Bannock and Portneuf Rivers; Rodgers et al. (2002) attribute this incision to greater subsidence of the ESRP than for valleys draining out onto the ESRP.

Recent detailed studies show the Tertiary history of normal faulting to be quite complex. Janecke et al. (2001) and Janecke (2007) subdivide normal faulting north of the ESRP and west of the Ruby graben (Fig. 9) into six phases of which they relate only the youngest phase to the

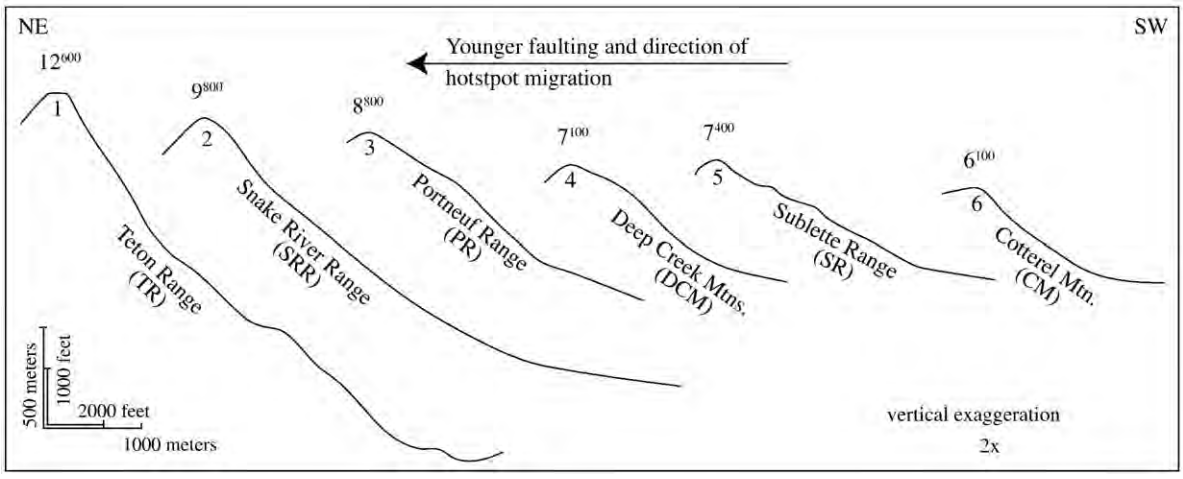

Fig. 12. Profiles of range fronts along southern side of the Yellowstone hotspot track showing reduction in both height and steepness of range front with distance back along the hotspot track. Profiles are from sites with a relatively planar (un-dissected) range front and where a relatively high peak is near the range front. In addition to the onset of fault activity being older from left to right, changes in the bedrock geology along the transect also influence the range front morphology. The Teton Range is in resistant Archean crystalline rocks, whereas the next 4 profiles are in sedimentary rocks of the Sevier thrust belt, and the westernmost profile is in late Cenozoic rhyolite. Total fault offset may also diminish from left to right. The locations of profiles and times of main fault offset are: Teton Range (TR) at Mt Moran (4.5 Ma to present), Snake River Range (SRR) at Baldy Mountain (5–2 Ma), Portneuf Range (PR) at Mt. Putnam (7–6.5 Ma), Deep Creek Range (DCR) at unnamed peak 8.5 km east of Rockland, Sublette Range (SR) at unnamed peak 3 km southeast of Hartley Peak, and Cotterel Mountain southwest of Horse Butte (10–>5 Ma). Faults may be on either the east or west sides of a range but the profiles here are drawn to descend to the right. 9^{800}-altitude of peak in thousands and hundreds of feet.

Yellowstone hotspot. In the Tendoy Range and Beaverhead Range and adjacent valleys (Fig. 9, TnR, BR), Janecke et al. (2001) map normal faults in the following categories: (1) older than the Challis Volcanic Group (49.5 Ma); (2) coeval with the Challis Volcanic Group (~49.5 to ~45 Ma); (3) mid-Tertiary major faults, mostly middle Eocene to Oligocene; (4) late to early Miocene faults with NE-trending strikes; (5) east-striking faults (younger than No. 3 and older than No. 6); and (6) active faults that generally strike NW and are commonly affected by the Yellowstone hotspot stress field. This complex extensional history makes it important to separate out deformation solely related to the Yellowstone hotspot. It generally holds that late Quaternary faults on major range fronts are hotspot related.

Most of the normal faults along the <10-Ma track of the Yellowstone hotspot (Fig. 9) have a westward dip which is the direction one might expect for westward gravity-driven extension from a landslide-like headwall. However, both the Teton and Centennial faults (Fig. 9) dip east and north respectively and away from the hotspot track. The dip of these two faults is compatible with the overall pattern of extension. These two faults are also where the hotspot has advanced into the craton and Precambrian igneous and metamorphic rocks are exposed in the footwall. The Sawtooth fault in central Idaho also dips northeast.

3.3.5. Tectonic and geomorphic changes in the area of the Ruby graben

On the north side of the ESRP, the Neogene Ruby graben records deformation correlated with the arrival in the area of the Yellowstone hotspot (Fig. 9, "Ruby graben") (Fritz and Sears, 1993; Sears and Fritz, 1998; Sears and Thomas, 2007). In Miocene time but prior to arrival of the hotspot, the northeast-trending Ruby graben was actively filling with sediment (Sixmile Creek Formation) (Sears et al., 2009-this volume) and the drainages trended northeast. The upper part of this basin fill contains the 6-Ma Timber Hill Basalt, which flowed 100 km north and then northeast along the graben from a vent most likely in the adjacent and then active Heise volcanic field (Morgan and McIntosh, 2005) on the ESRP (Fig. 9) (Fritz et al., 2007). Then, shortly after 6 Ma, the orientation of normal faulting changed by 90° from a northeast to a northwest strike, with extension reoriented SW–NE as is manifest in ranges farther to the SW (Tendoy, Beaverhead, Lemhi, and Lost River Ranges) (Fig. 9). The shift in fault trends correlates with the northeast advance into the area just south of the Ruby graben of hotspot volcanism of the 6.62-Ma Heise volcanic field and associated hotspot-swell uplift (Sears and Fritz, 1998; Sears and Thomas, 2007).

3.4. Uplift and subsidence

3.4.1. Hotspots typically are associated with a broad topographic swell 1–2 km high and roughly 1000 km across (Crough, 1983; see Saunders et al., 2007)

The Yellowstone Crescent of High Terrain (YCHT) is a high-altitude, parabola-shaped highland that heads on the leading margin of the hotspot track and flares outward about the volcanic track (Fig. 9) (Pierce and Morgan, 1992, Plate 1). Two altitudinal parameters support a deep (mantle) origin for the Yellowstone hotspot track: 1) The leading margin of the YCHT is 100 km northeast of and in advance of the progression of hotspot volcanism (Fig. 9), and 2) the Yellowstone geoid anomaly has an outer (leading) margin 200–250 km northeast of and in advance of Yellowstone volcanism and has a hotspot-swell-like character (Fig. 9, inset map).

Molnar and England (1990a,b) persuasively argue that late Cenozoic incision generally results from enhanced erosion resulting from ice-age climates rather than non-isostatic uplift. For many areas being actively incised their argument is supported by the lack of a plausible geophysical mechanism to activate uplift. But, in the case of the Yellowstone hotspot track, a mantle plume provides a reasonable explanation for uplift. Ten lines of evidence support interpretation of the YCHT as a swell-like uplift fitting the plume-tail model (Pierce and Morgan, 1992; Saunders et al., 2007). We here describe six lines of evidence for uplift and then list four more.

3.4.2. Geoid

The highest part of the geoid in the conterminous United States is centered just northeast of the Yellowstone Plateau (Fig. 9, inset map). In contrast, the largest Bouguer and altitude anomalies center in western Colorado with Yellowstone being only a bench on this larger anomaly. Because the compensation depth for the geoid anomaly is deeper than that for the Bouguer anomaly, a deep-seated process centered under Yellowstone must be involved. No geologic process other than a deep mantle plume readily explains this Yellowstone geoid anomaly. The geoid anomaly also supports the interpretation of young uplift of the YCHT. Lowry et al. (2000) conclude that "The largest of the significant dynamic elevation anomalies [in the western U.S.] is consistent with that predicted by numerical modeling of the Yellowstone hotspot swell."

3.4.3. Contrasting terrace sequences

In the ESRP along the trailing margin of the hotspot track, only low river terraces are present and are typically of last glacial and younger age (younger than 25,000 years). In contrast, high stairsteps of terraces (terrace flights) spanning back to 1 Ma or older occur in the Wind River and Bighorn basins on the leading edge of the hotspot. This difference may be explained by uplift producing high terrace flights on the leading margin of the hotspot swell whereas subsidence results in only young, low terraces on the trailing margin and related to the latest Quaternary glacial–interglacial climate changes.

3.4.4. Tilted Wind River terraces

The "bow wave" pattern of the YCHT is predicted to produce tilting away from Yellowstone. The tilts can be quantified using two well-dated Quaternary terraces of the Wind River, located 200 km southeast of Yellowstone (Figs. 9 and 13). Over a distance of 90 km, the older terrace increases in height towards Yellowstone by 30 m more than does a younger terrace (Fig. 13). Lava Creek tephra dates the older terrace at 640-ka (Jaworowski, 1994) and U-series ages on soil-carbonate clast coatings date the younger Bull Lake terrace at 150 ka (Sharp et al., 2003), giving an age difference of 490 k.y. (~0.5 m.y.). The leading edge of the geoid anomaly is ~200 km from the track centerline, which with a hotspot motion of 25 km/m.y. would span an uplift interval of 8 m.y. Assuming straight-lever geometry of tilting, a rough magnitude of the total uplift is estimated as:

30 m × 16 × 2.2 = 1056 m (rounded to 1 km), where
16 = Total uplift interval (8 m.y.) divided by interval sampled (0.5 m.y.)
2.2 = Total length of uplift (200 km) divided by terrace length sampled (90 km)

This total of 1 km uplift over 8 m.y. converts to an uplift rate of ~0.1 mm/yr (0.125 mm/yr).

3.4.5. Pinedale to Bull Lake glacial–length ratios

In the Rocky Mountains, the lengths of valley glaciers during the Pinedale glaciation (Pd, ~20 ka) were typically 90–95% of those in the same valley during the Bull Lake glaciation (BL, ~140 ka). If uplift occurred in the YCHT during the interval between glaciations, the size of Pinedale glaciers would increase above what would be their size without uplift, and thus the ratio of Pinedale to Bull Lake glacier lengths (Pd/BL ratio) would also increase to larger than the typical 90–95% ratio for the Rocky Mountains. The converse would be the case if subsidence occurred. On the leading margin of the YCHT, the Pd/BL ratio is commonly about 100% or more. A calculation of the equilibrium line altitude (ELA) change consistent with a 5–10% increase in Pinedale glacier length is 20–40 m (see Pierce and Morgan, 1992, p. 23). Such an altitude change over the 120 k.y. time interval

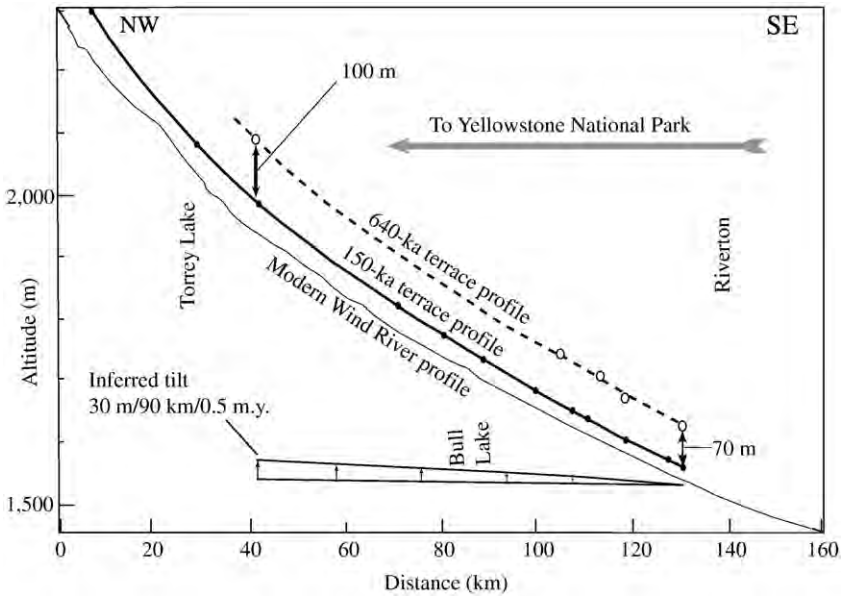

Fig. 13. Tilting of terraces of the Wind River away from Yellowstone (after Jaworowski, 1994) (see Fig. 9 for location). Profiles of two dated terraces along the Wind River south of Yellowstone diverge by 30 m upstream towards the Yellowstone area over a distance of 90 km. This inferred tilting occurred over an interval of ~0.5 Ma. Based on plate-tectonic motion and the leading margin of the geoid anomaly, the total uplift interval is ~8 Ma. This yields uplift on the leading margin of the Yellowstone Crescent of High Terrain totaling about 1 km at a rate of ~0.1 mm/yr.

yields an estimate of uplift rates between 0.1 and 0.4 mm/yr (0.17 to ~0.33 mm/yr).

3.4.6. Uplifted 2.05-Ma Tuff

The 2.05-Ma Huckleberry Ridge Tuff ramps up on the YCHT to altitudes 500 to 1000 m higher than its altitude around the western part of its source caldera (Christiansen, 2001). This difference combines uplift on the YCHT with subsidence on the hotspot's trailing margin. The elevation difference over the past 2 m.y. yields a change of 0.25 to 0.5 mm/yr. If subsidence and uplift are equal, then uplift would be between 0.1 and 0.3 mm/yr (0.12 and 0.25 mm/yr).

3.4.7. Uplift, incision, and high mountains of erodible rocks

On the leading margin of the hotspot track 40 km northeast of the 0.64-Ma Yellowstone caldera, a gently rolling upland is incised about 1 km (Fig. 14). At a location southeast of the 0.64-Ma caldera, a 3.6-Ma basalt on this upland surface predates incision of this surface (Ketner et al., 1966; Blackstone, 1966). Similarly, gravel now perched on the upland surface contains clasts of 6.26 ± 0.06-Ma obsidian (Naeser et al., 1980), emplaced before dissection of this surface. This obsidian may be from a local upper Tertiary rhyolite (Smedes et al., 1989), or possibly even from the Walcott Tuff (6.27 ± 0.04 Ma) (Morgan and McIntosh, 2005). Near the axis of the YCHT, mountain peaks and glacial cirques are formed of easily eroded Eocene volcanic breccias and Mesozoic sandstone and shale. These readily erodible peaks could not remain so high for long, indicating that young uplift has occurred. Incision of 1000 m after eruption of the 3.6-Ma basalt yields an incision rate of 0.3 mm/yr.

3.4.8. Summary of uplift rates and other uplift indicators

Based on the above four estimates (Sections 3.4.4, 5, 6, 7), uplift rates are but a low fraction of a millimeter a year (0.1 mm to 0.4 mm),

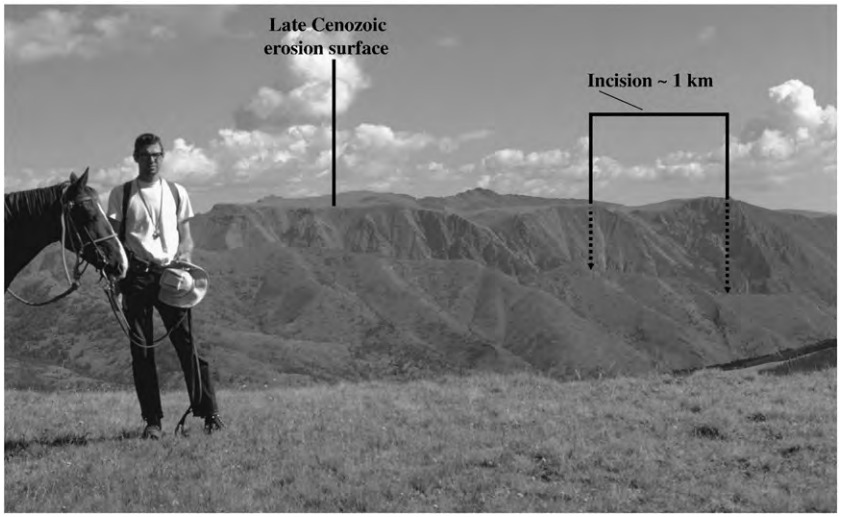

Fig. 14. Photograph showing young incision of upland surface on leading margin of YCHT. Picture taken from eastern boundary of Yellowstone Park looking eastward to Hurricane Mesa, a flat topped late Cenozoic erosion surface formed on Eocene volcanic rocks. The intervening valleys were incised as much as 1 km in late Cenozoic time. Further south, incision of the erosion surface is dated 4 to 6 Ma (see text).

but over say 5 m.y. could result in 0.5 to 2 km of uplift. These rates are useful to estimate the GPS resolution that is needed to measure uplift and subsidence of the YCHT.

Some additional indicators of possible uplift are: (Pierce and Morgan, 1992):

(1) Repeat leveling across the YCHT shows an arch of uplift highest near the crest of the YCHT.

(2) In the Big Horn Basin (Fig. 9) on the leading (northeast) margin of the hotspot, older terraces are tilted away from Yellowstone both for streams flowing away from Yellowstone (terraces diverge upstream) and for streams flowing towards Yellowstone (terraces converge upstream). This geometry requires uplift and tilting away from Yellowstone on the leading margin of the YCHT.

(3) Also on the leading margin of the hotspot, the terrace sequence of the Bighorn River descends so that lower, younger terraces are to the east, consistent with tilting away from Yellowstone.

(4) Rock Creek flows away from Yellowstone in southern Montana (Fig. 9). Longitudinal terraces profiles for its terrace sequence show a pattern of downvalley convergence and then divergence so that the convergent–divergent location between successively younger terraces steps away from Yellowstone consistent with a concavity (flexure) associated with hotspot uplift migrating northeast at a rate similar to the ~25 km/m.y. movement of the North American plate.

3.5. Asymmetry of the hotspot track and upper mantle winds

A marked topographic and tectonic asymmetry is associated with Phase III (10 Ma to present) of the Yellowstone hotspot track (Pierce and Morgan, 1992, 2005). Asymmetry across the ESRP is shown by mapped patterns of faulting and the YCHT that both flare out in a bow wave-like pattern away from the Yellowstone-volcanic-track centerline. For example, fault Belt II flares out 1.6 times more on the south side of the track than on the north (Fig. 9). Much of the area of this asymmetric flaring is accounted for by the pie-shaped area of fault Belt IV (major late Tertiary or early Quaternary faults), which is only on the south side of the ESRP. The YCHT is also asymmetric: the axis of the crescent extends ~1.5 times farther south than north about the hotspot track (Fig. 9). Asymmetry also is reflected in the distribution of the young basaltic vents and rift zones that are concentrated along the northern margin of the plain, commonly oriented with a north–northwest trend. This asymmetry may be significant and the finding that the Yellowstone plume rises up to the southeast to intercept Yellowstone (Yuan and Dueker, 2005; Waite et al., 2006) may be related to this track asymmetry.

In looking for a possible connection between the inclined Yellowstone plume and the asymmetrical pattern of faulting, uplift, and recent basaltic volcanism, we note the following.

1) The North American plate motion has been at a direction and velocity compatible with that of the volcanic hotspot track progression over the last 10 Ma (N55°E, at ~25 km/m.y.) and is about at a right angle from the southeast rise direction of the inclined plume suggesting that this geometry may extend back 10 or more million years.

2) Hot fluids associated with a plume rising from 500 km depth inclined 20° from vertical and at a position 170 km NW of Yellowstone might be thought to rise convectively more nearly vertical and heat the rock vertically above, which would make the northern zone of faulting and uplift wider. However, the northern side is not wider but narrower. If upper mantle flow, known as mantle winds, is tilting the plume, then the upward rise of the plume would be in the moving "reference frame" of the mantle wind and tilt with that wind.

3) Faulting Belt IV on the southern side of the ESRP may be farther from the thermal influence of the inclined plume and also above stagnant higher-velocity residuum (restite) that was swept southeastward to the far side of the inclined plume. Humphreys et al. (2000) note higher velocity material interpreted as residuum in this area south of the ESRP, but also noted such material north of the ESRP.

Mantle winds can readily explain the rise of the mantle plume to the southeast. Three models of upper mantle flow yield an east–northeast rise, but the Berkeley model (SAW24B16k) yields a rise to the southeast (Bernhard Steinberger, 2000; written commun., 2005; Pierce and Morgan, 2005). Waite et al. (2006) considered easterly upper mantle flow was involved in the SE rise of the Yellowstone plume, but also thought that the Madison mylonite zone north of the hotspot track might provide a weakness into which the plume was deflected. Because the Madison Mylonite zone trends along a line that is about 60 km northwest of the hotspot track but was not exploited by the hotspot track, we concluded that the track is controlled by processes below the lithosphere (Pierce and Morgan, 1992). For the area several hundred kilometers west of Yellowstone, Zandt and Humphreys (2008) suggest the Vancouver slab, bounded by a slab window to the south, sets up toroidal flow in the upper mantle that explains the inferred orientation of olivine in the upper mantle of the northern Nevada region, but such torridal-flow pattern does not extend as far east as the ESRP and Yellowstone area.

Shervais and Hanan (2008) explain tilting of the plume tail to be the result of the plume head being sheared off by the cratonic lithosphere, and the rising plume tail tilting southeast towards a thermally eroded channel in thin lithosphere beneath the central SRP about 12 Ma. They conclude that, once established, this channel controls the present tilt of the plume.

3.6. Three overarching processes spanning the entire 17–0 Ma hotspot track

We discuss here three processes relevant to a mantle plume hypothesis that span all or much of the hotspot track. We first describe drainage changes, which are the most complex to describe and a fruitful field for continued studies such as done by Paul Link and students (Link et al., 1999, 2002, 2005; Beranek et al., 2006; Hodges et al., 2009-this volume). We then discuss high $^{3}He/^{4}He$ ratios and lastly the depth of the inferred mantle plume.

3.6.1. Drainage changes associated with the hotspot track

Modern streams flow radially outward from Yellowstone (Fig. 15), reflecting doming centered on Yellowstone that is consistent with uplift above a mantle plume beneath Yellowstone. The Continental Divide crosses through the center of this radial pattern (Figs. 15 and 16D). On the trailing edge of the hotspot track, the lowland ESRP is drained by the Snake River whose watershed divide itself is consistent with its control by processes associated with the northeastward-migrating Yellowstone hotspot (Wegmann et al., 2007).

In Oligocene time, the Continental Divide "mostly lay only a few hundred km inland from the Pacific coast" (Hamilton, 1999), which is a thousand kilometers west of its present position in Yellowstone. Given this present drainage pattern, it has been suggested that similar patterns of drainage, local divides, and the Continental Divide may have accompanied more westward, older positions of the hotspot (Pierce and Morgan, 1992; Fritz and Sears, 1993; Sears and Fritz, 1998; Link et al., 1999; Pierce et al., 2002; Wood and Clemens, 2002; Link et al., 2005; Beranek et al., 2006; Hodges 2006; Wegmann et al., 2007; Stroup et al. (in press).

The 16-to-2-Ma progression of hotspot volcanic fields and inferred drainage divides and stream-flow directions (Fig. 16) were compiled from multiple sources. Following the work by Link et al. (2005) that established the reproducibility of detrital zircon signatures for streams with distinct provenance in the Snake River system, Beranek et al. (2006) examined Miocene and Pliocene fluvial sediments of the western Snake River Plain to determine when the west-flowing Snake River developed. Fig. 16 shows drainage flow direction at four different time intervals. From these data, we have inferred locations of drainage divides between the Snake and Missouri River system on the north and the Bonneville Basin on the south. North of the hotspot track this divide commonly coincides with the paleo-Continental

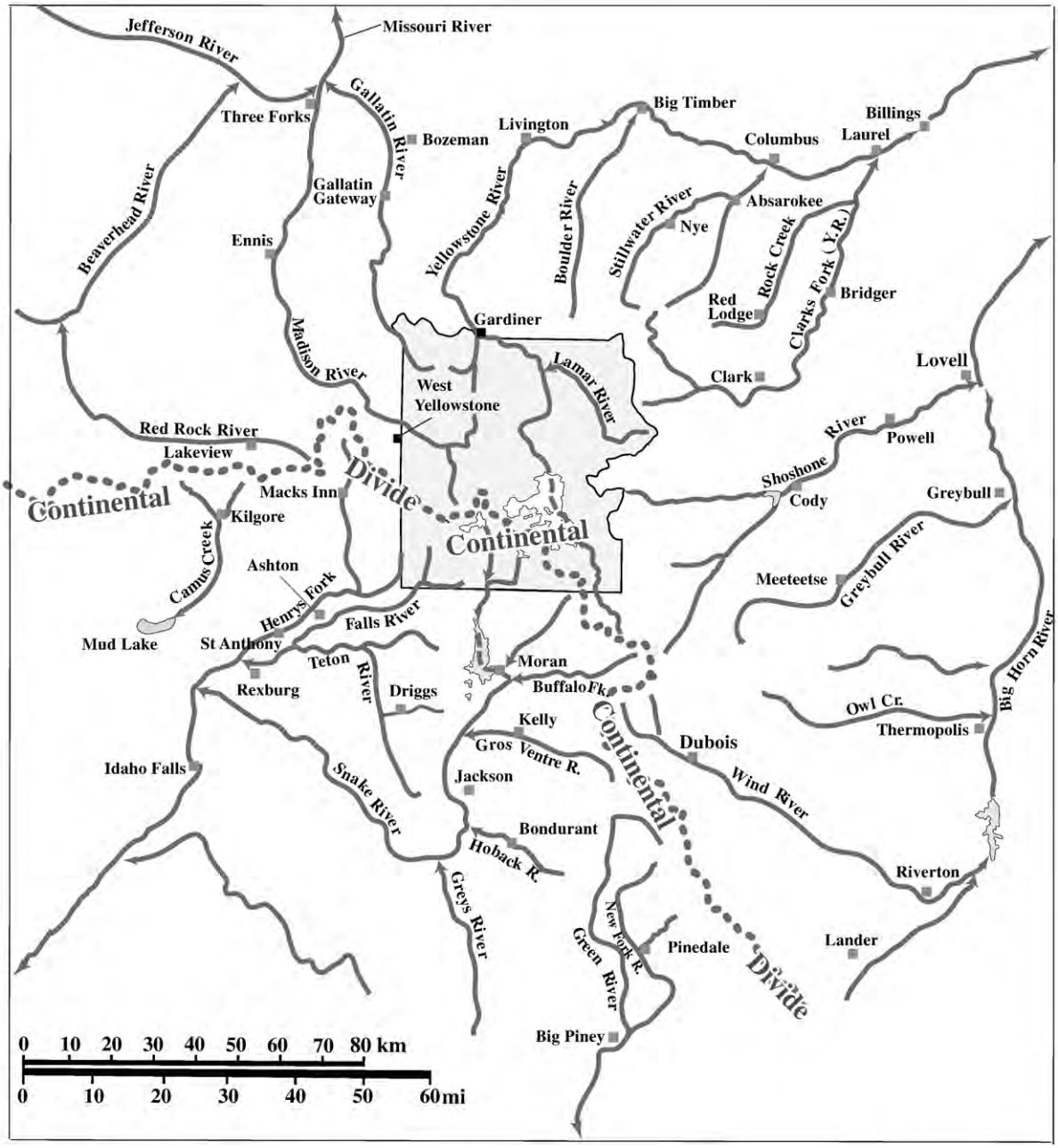

Fig. 15. Radial drainage pattern outward from the present position of the Yellowstone hotspot, suggesting uplift. The Continental Divide (short dashed gray line) is also associated with the Yellowstone hotspot. Note the tendency towards a circular pattern towards the margin of the figure, as pointed out by Michael Machette (written commun. 2008).

Divide and south of the track are divides within basin and range half-grabens separating southward flow into the eastern Great Basin from northward drainage into the developing Snake River Plain. There is a progressive eastward shift of drainage divides from western Idaho to western Wyoming (Fig. 16), although reconstructions are not nearly as well defined as the present radial pattern (Fig. 15).

For the flood basalts near the Oregon–Idaho border (Fig. 16A, near 16 [Ma] in star), we show a northward drainage as supported by the northerly migrating sequence of flows discussed in Section 3.1.2 (Camp and Ross, 2004). This is consistent with a radial pattern of drainage outward from the center of the inferred plume head as well as northward directed compression to produce the Yakima folds and thrust belt near the Oregon–Washington state boundaries (Hooper, 1990; Pierce et al., 2002, Fig. 6).

In the 16–15 and 10–8 Ma intervals, detrital zircons from the central and eastern Idaho thrust belt were not carried to deposits in the western Snake River Plain (Beranek et al., 2006) indicating an ancestral Snake River divide migrating to somewhere near the present location of the 11-to-10-Ma volcanic fields (Fig. 16A,B). At about 7 Ma, the divide migrated eastward and such zircons now were carried to the western SRP. Based on evidence for an increase of the level of Lake Idaho in the western SRP at ~6 Ma, Wood and Clemens (2002) also conclude that the divide migrated eastward and thereby enlarged the runoff from the upper Snake River.

The Ruby graben preserves deposits with material documenting a 6-Ma drainage northeastward along the present hotspot track (Fig. 16C). This stream flow pattern is based on both diagnostic lithologies from central Idaho as well as 9–12 Ma zircons from deposits in the Picabo or older volcanic fields (Sears and Thomas, 2007; Stroup et al., 2008a,b; Sears et al., 2009-this volume).

After 10 Ma, flow may have continued eastward and perhaps southward towards the Bonneville Basin (Fig. 16B, C). Mollusk distributions

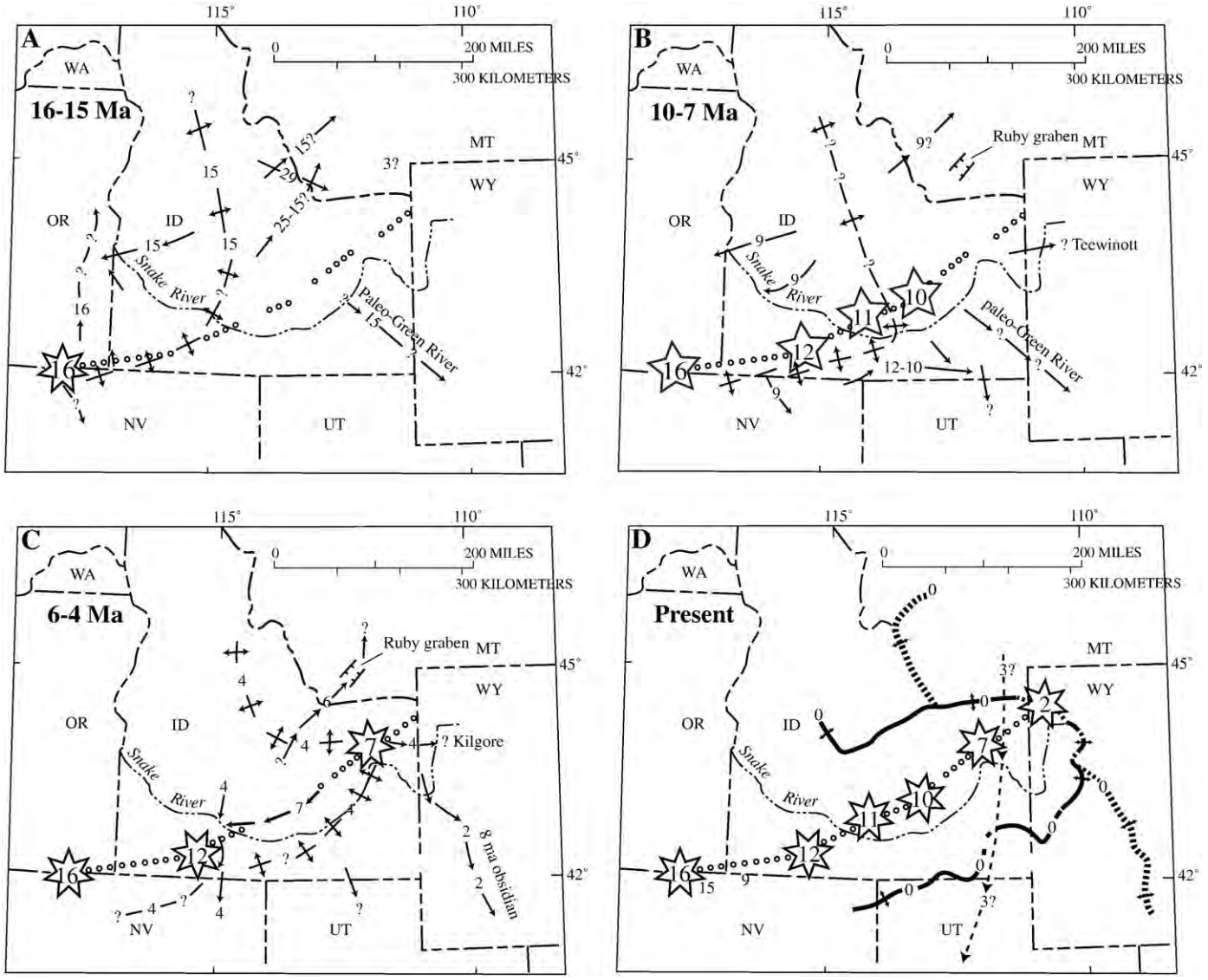

Fig. 16. Sketch maps for the last 16 Ma along the Yellowstone hotspot track showing changes in stream-flow directions and eastward shift of drainage divides. The arrows indicate stream flow direction with numbers indicating approximate ages in million years ago (Ma). Dashed line crossed by outward pointing arrows — inferred drainage divide. The track of the Yellowstone hotspot is shown by line of small, open circles. Some of the rhyolitic volcanic fields are designated by stars with their inception ages given in Ma (million years ago). Reconstructions mostly from Beranek et al. (2006) based on methods substantiated by Link et al. (2005). Additional stream and divide references are given under time-intervals A to D. (A) About 15–16 Ma at the time of inferred plume-head uplift. A northward slope from the 16 Ma rhyolite center is based on northward progression of flood basalts down the northward migrating bulge (Camp and Ross, 2004). The northeast-flowing stream at 25-15? Ma from Hailey, Idaho to Dillon, Montana is based on Stroup et al. (in press), whereas the southeast flowing stream into SW Montana at 29 Ma is based on Hodges (2006); (B) About 10–7 Ma. The headwaters of the paleo-Snake River were located somewhere near the 10–11 Ma volcanic centers because detrital zircons from the central and eastern Idaho thrust belt are absent in western SRP deposits prior to 7 Ma. Stream course at 12 to 10 Ma near the Idaho–Utah border is based on eastward transport of 15–10 Ma hotspot volcanic zircon grains and 10 Ma volcanic glass to the Malad Range near the Idaho–Utah border (Long et al., 2006); (C) About 4–6 Ma. Eastward migration of the Snake River divide to 7 Ma volcanic center based on detrital zircons from the central and eastern Idaho thrust-belt, and zircons in <7 Ma strata in the western SRP (Beranek et al., 2006). Based on a rise of Lake Idaho ~6 Ma, Wood and Clemens (2002) also postulated an eastward expansion of the Snake River drainage. Stream flow from central Idaho into the Ruby graben includes distinctive gravel lithologies (Sears et al., 2009-this volume); and (D) Present Snake River and its drainage divides. Short dashed line with 0 — Continental Divide. Heavy line with 0 — both Continental Divide and present Snake River drainage divide. The association of the Snake River and its drainage divides with the Yellowstone hotspot track strongly supports the eastward expansion of the Snake River drainage that followed subsidence of the Snake River Plain after passage of the Yellowstone hotspot. Wegmann et al. (2007) quantitatively analyzed this relation.

support flow southward into the Bonneville Basin between 9–5 Ma (Fig. 16B, south arrow on Utah–Idaho state line) (Taylor and Bright, 1987). Wood and Clemens (2002) conclude that the Snake River acquired greater runoff by capturing terrain east of this position after 6–7 Ma and before 5.5 Ma.

Studies of late Cenozoic fish reflect a complex history of drainage changes along the track of the Yellowstone hotspot. The Late Miocene–Pliocene(?) paleo-Yellowstone River apparently headed near the position of Pocatello, Idaho and drained northeast to the Hudson Bay (Smith, 1981; Smith and Patterson, 1994), consistent with drainage directions also indicated by both detrital zircon ages and diagnostic chert grains transported northwest to deposition in the Ruby graben (Stroup et al., 2008a,b; Sears et al., 2009-this volume).

About 50 km east of the Ruby Graben at a fish hatchery in the Madison Valley (Fig. 16D, long dashed arrow to south), a contrasting Pliocene (?) reconstruction of southward stream flow is based on snail species in the present upper Missouri River Basin (*Pyrgulopsis blainica*) connected south across the Continental Divide into the Great Basin where extensive populations of very closely related form *P. anguina*, occur (Hershler et al., 2008). Based on molecular clock rates, the time when these drainages were connected was about 3 Ma. This drainage reconstruction seems incompatible with the Ruby

graben geologic data that indicate northeastward stream flow sourced 200 km to the southwest of the graben (Fig. 16C). For a southward (not northward) drainage across the present Continental Divide to be present one or more of the following are required: (1) multiple stages of stream capture are involved; (2) the age of the upper Missouri connection needs to be perhaps 3 times older than the "molecular clock" age; and (3) there was a drainage that flowed south from the Madison Valley, across the present Reynolds Pass and through the Henrys Lake area to the upper Island Park area. Alternatively, the snails at the fish hatchery site in the Madison Valley might have been historically introduced. Distribution of the worm (*Rhynchelmis gustafsoni*) studied by Dan Gustafson (personal commun., 2008) provides conclusive evidence that the Madison Valley and upper Henrys Fork area were once connected and drained either to the north or south.

Paleo-vegetation studies have the potential of constraining altitude and subsidence along the hotspot track (Davis et al., 2006). Preliminary studies show much wetter environments along the hotspot track (eastern Snake River Plain) in late Cenozoic time than at present, indicating change in either regional–global climate, or, we suggest, higher altitudes in the past (Davis et al., 2006).

3.6.2. High $^3He/^4He$ ratios

The Yellowstone hotspot track has anomalously high $^3He/^4He$ ratios (Kennedy et al., 1987; Craig, 1997; Dodson et al., 1997; Graham et al., 2007, 2009-this volume). The origin of the high $^3He/^4He$ ratios is debated (see discussion in Graham et al., 2009-this volume), but ratios well above 8 R_A (8 times the ratio in the atmosphere) are commonly thought to indicate a deep mantle source (Kurz et al., 1982; Gonnermann and Mukhopadhyay, 2007). North of Yellowstone, olivine phenocrysts from the 2-Ma Emigrant Basalt have $^3He/^4He$ ratios >21 R_A (Mark Kurz and Joe Licciardi, written commun., 2007). Similarly, olivine phenocrysts from basalts from the ESRP have $^3He/^4He$ ratios that increase from >13 R_A in the western part of the SRP to >19 R_A near Yellowstone and are attributed to a plume source (Graham et al., 2007, 2009-this volume). Olivine phenocrysts from the Imnaha Basalt (Columbia River Basalt Group) have $^3He/^4He$ ratios of 11.4 R_A that Dodson et al. (1997) attribute to the Yellowstone plume. As discussed earlier in the delamination scenario for the Steens and Columbia flood basalts by Camp and Hanan (2008), the Imnaha Basalt has geochemistry indicating the highest contribution from decompression melting of the Yellowstone plume.

3.6.3. Depth of origin of Yellowstone plume

Although published geophysical studies can only trace an inclined plume beneath Yellowstone to a depth of ~500 to 660 km (Yuan and Dueker, 2005; Waite et al., 2006; Smith et al., 2007), we suggest the following system scaling factors favor a deeper origin (Pierce et al., 2007): (1) the starting plume head occupied the thickness of the upper mantle, and assuming a 500–660-km depth for the plume, this configuration does not fit the plume head-tail model where the bottom of the plume head rises buoyantly as it is inflated by the plume tail in that the head bottom stays at the base of the upper mantle (Fig. 5); (2) the YCHT and the belts of faulting are ~400 km across; and (3) the geoid anomaly is 800 km across, much wider than the 500 km imaged depth of the mantle plume. Thus a large potential source is involved, and it seems out of proportion that the geoid anomaly and the YCHT be driven by a relatively shallow process. The history of the hotspot indicates a sustained, large-scale process on a scale of many hundreds of kilometers across at the earth's surface and with a comparable or deeper depth scale that has been active over the past 16 m.y.

New information is emerging regarding the depth of the Yellowstone plume. Allen et al. (2008) conclude "The narrow low velocity conduit beneath Yellowstone National Park dips to the northwest in the upper mantle and connects to a much broader low-velocity anomaly in the uppermost lower mantle." A tomographic image, courtesy of Richard Allen, showing a plume extending to more than 1000 km is published in Lay (2009, image on page 46). This low-velocity body is below and larger than the upper mantle plume imaged by Yuan and Dueker (2005) and Waite et al. (2006) and appears to be the heat source for the plume recognized from the transition zone upward.

The core–mantle boundary is the most reasonable source of heat to drive a thermal mantle plume (Hill et al., 1992; Sleep, 2006; Campbell, 2007; Lay et al., 2008). Other heat sources are more complex, but Courtillot et al. (2003) conclude that plumes may also arise from the bottom (660 km) and top of the transition zone (440 km).

Although the tomographic studies of Yuan and Dueker (2005) and Waite et al. (2006) conclude the thermal anomaly or plume beneath the Yellowstone caldera extends to only ~500 km depth, studies underway (see above) favor a source below the transition zone. We note that until recently a plume extending even to 500 km was not geophysically imaged until a wider tomographic array was acquired and analyzed. Schubert et al. (2001) note that "… lower mantle plumes may be so altered by the transition zone that they appear to originate from within it." Fee and Dueker (2004) find no upward deflection of the 660 discontinuity for the Yellowstone plume. Although a lower mantle plume is predicted to elevate the 660-km discontinuity due to the negative Clapeyron slope for the post-spinel change, for a hot plume, the majorite/garnet phase transformation has a positive Clapeyron slope which would lower the 660-km discontinuity; the combined effect might reduce or eliminate upward deflection of the 660-km discontinuity (Hirose, 2002). Tauzin et al. (2008) find "no clear evidence for a thin [necked down] transition zone beneath hotspots and that "The depth of the 660-km discontinuity may be less temperature sensitive in hot regions of the mantle, which is consistent with the effect of a phase transition of the majorite–garnet to perovskite at a depth of 660 km".

4. Summation and comments

The imaging of an inclined mantle plume beneath Yellowstone supports the conclusion that the entire Yellowstone hotspot track was driven by a mantle plume, including its inception with a plume head 17 Ma. Support of a plume head origin of the track includes: (1) flood basalt volcanism, including a northward spreading plume head and postulated delamination that explains flood basalt differences; (2) coeval rhyolite volcanism to the south through generally more cratonic crust; (3) extension following rather than preceding volcanism; (4) a large mass deficit; and (5) coeval mineralization. We need better understanding of the following: (1) the size of the plume head and its depth of origin; (2) coeval Basin and Range extension but which centers well to the south of the center of the plume head; (3) whether or not the lithosphere thickens eastward across the cratonic boundary; (4) plume interaction with the Juan de Fuca slab; and (5) 17–10 Ma hotspot migration rates 2.5 times too high for plate motion.

The transition (14 to 10 Ma) from plume head to plume tail involves volcanism characterized by high eruptive volumes, high temperatures, and a large number of eruptions scattered throughout an east–west band ~200 km wide. There is little documentation for faulting and uplift that may be associated with this transition; further study is needed.

The plume-tail phase (10–0 Ma) has volcanic fields starting with calderas 10.21, 6.62, and 2.05 Ma. They delimit a track moving N 55° E at 29 km/m.y. (~24 km/m.y. corrected for extension), which is similar to the motion of the North American plate. The Yellowstone Crescent of High Terrain (YCHT) flares out in a bow wave-like pattern about the volcanic track and heads in front of the volcanic progression favoring a sub-lithosphere driver. Uplift estimates of YCHT are between 0.1 and 0.4 mm/yr. The Continental Divide as well as a radial drainage pattern now center on Yellowstone as does the largest geoid anomaly in the conterminous U.S. For the last 17 Ma, flow direction of drainages and position of divides has changed consistent with uplift and subsidence associated with northeast migration of doming associated with the Yellowstone hotspot.

Bands of late Cenozoic faults flare outward from the hotspot track generally on the inner slope of the "bow wave" of the YCHT where there is a gravitational potential for extension to the west. High fault activity has migrated in tandem with the volcanic hotspot. Classification of faults by recency of offset and range-front height is compatible with a parabolic "wave" of fault activity that also has migrated northeastward.

The belts of faulting and the crest of the YCHT are asymmetrical about the hotspot track but flare outward ~1.6 times further on the south side of the hotspot track. The southeast rise of the Yellowstone plume and this asymmetry might both reflect southeast flow of the upper mantle.

We have argued that the track of the Yellowstone hotspot is best explained by a plume driven from the core–mantle boundary. The size of the inferred plume head favors a source below the transition zone. Early geophysical studies did not identify a plume deeper than ~200 km; later instrumentation and broader arrays identified a plume extending to only about 500 km. Current geophysical techniques apparently can now extend a plume to a depth of at least 1000 km. We think the scale at the earth's surface of volcanism, faulting, and uplift is best explained by a source in the lower mantle. In summary, the interaction between a likely mantle plume and the moving North American plate provides a 17-Ma geologic laboratory amenable to integrated topical studies over a several state area, including volcanism, faulting, geomorphology, and uplift.

Acknowledgments

We thank Mike Machette, Vic Camp, Paul Link, Henrietta Cathey, and Dennis Geist for their helpful reviews. Paul Link kindly twice reviewed and shared his knowledge for the section on drainage changes. We appreciate rewarding discussions and emails with Richard Allen, Mark Anders, Vic Camp, Bob Christiansen, Ken Dueker, Irv Friedman, Bill Fritz, John Good, Alice Gripp, Hank Heasler, Gene Humphreys, Cheryl Jaworowski, Karl Kellogg, Dave Lageson, Bill Leeman, Mike Machette, Barbara Nash, Susan Olig, Tom Parsons, Jennifer Pierce, Jack Reed, Marith Reheis, Dave Rodgers, Cal Ruleman, Bernhard Steinberger, Rick Saltus, Derek Schutt, Jim Sears, Pat Shanks, Betty Skipp, Norm Sleep, Bob Smith, Mike Stickney, Benoit Tauzin, George Thompson, Alan Wallace, and Huaiyu Yuan. Mary Berger capably drafted the illustrations and Ken's wife Linda encouraged the undertaking.

References

Allen, R.M., Xue, M., Hung, S., 2008. Complex geological interactions in the mantle beneath western USA. Eos Transactions, American Geophysical Union: Fall Meeting Supplement, Abstract S31D-02, vol. 89(53).

Anders, M.H., 1994. Constraints on North American plate velocity from Yellowstone hotspot deformation field. Nature 369, 53–55.

Anders, M.H., Geissman, J.W., Piety, L.A., Sullivan, J.T., 1989. Parabolic distribution of circum-eastern Snake River Plain seismicity and latest Quaternary faulting: migratory pattern and association with the Yellowstone hot spot. Journal of Geophysical Research 94, 1589–1621.

Anderson, D.L., 1994. The sublithospheric mantle as the source of continental flood basalts: the case against the continental lithosphere and plume head reservoirs. Earth and Planetary Science Letters 123, 269–280.

Anderson, D.L., 1998. The helium paradoxes. Washington, D.C. Proceedings National Academy of Sciences 95, 4,822–4,827.

Anderson, D.L., 2000. The thermal state of the upper mantle; no role for mantle plumes. Geophysical Research Letters 27, 3,623–3,626.

Armstrong, R.L., Leeman, W.P., Malde, H.E., 1975. K–Ar dating, Quaternary and Neogene rocks of the Snake River Plain, Idaho. American Journal of Science 275, 225–251.

Atwater, T., 1989. Plate tectonic history of the northeast Pacific and western North America. In: Winterer, E.L., Hussong, D.M., Decker, R.W. (Eds.), The Eastern Pacific Ocean and Hawaii. The Geology of North America, vol. N. Geological Society of America, pp. 21–72.

Baksi, A.K., 1989. Reevaluation of the timing and duration of extrusion of the Imnaha, Picture Gorge, and Grande Ronde Basalts, Columbia River Group. In: Reidel, S.P., Hooper, P.R. (Eds.), Volcanism and Tectonism in the Columbia River Flood Basalt Province: Geological Society of America Special Paper, vol. 239, pp. 105–111.

Beranek, L.P., Link, P.K., Fanning, C.M., 2006. Miocene to Holocene landscape evolution of the western Snake River Plain region, Idaho: using the SHRIMP detrital zircon provenance record to track eastward migration of the Yellowstone hotspot. Geological Society of America Bulletin 118, 1027–1050.

Blackstone, D.L., 1966. Pliocene volcanism, southern Absaroka Mountains, Wyoming: Laramie, University of Wyoming. Contributions to Geology 5, 21–30.

Bohannon, R.G., Parsons, T., 1995. Tectonic implications of post-30 Ma Pacific and North American relative plate motions. Geological Society of America Bulletin 107, 937–959.

Bonnichsen, B., Kaufman, D.F., 1987. Physical features of rhyolite lava flows in the Snake River Plain volcanic province, southwestern Idaho. Geological Society of America Special Paper 212, 119–145.

Bonnichsen, B., Godchaux, M.M., 2002. Late Miocene, Pliocene, and Pleistocene geology of southwestern Idaho with emphasis on basalts in the Bruneau–Jarbidge, Twin Falls, and western Snake River Plain regions. In: Bonnichsen, Bill, McCurry, M., White, C.M. (Eds.), Tectonic and Magmatic Evolution of the Snake River Plain–Yellowstone Volcanic Province: Idaho Geological Survey Bulletin, vol. 30, pp. 233–312.

Bonnichsen, B., Leeman, W.P., Honjo, N., McIntosh, W.C., Godchaux, M.M., 2007. Miocene silicic volcanism in southwestern Idaho: geochronology, geochemistry, and evolution of the central Snake River Plain. Bulletin of Volcanology 70, 315–342 (published online 2007).

Braile, L.W., Hinze, W.J., von Frese, R.R.B., Keller, G.R., 1989. Seismic properties of the crust and uppermost mantle of the conterminous United States and adjacent Canada. In: Pakiser, L.C., Mooney, W.D. (Eds.), Geophysical Framework of the Continental United States: Geological Society of America Memoir, vol. 172, pp. 655–680.

Burov, E., Guillou-Frottier, L., d'Acremont, E., Le Pourhiet, L., Cloetingh, S., 2007. The plume head–lithosphere interactions near intra-continental plate boundaries. Tectonophysics 34, 15–38.

Camp, V.E., 1995. Mid-Miocene propagation of the Yellowstone mantle plume head beneath the Columbia River Basalt source region. Geology 23, 435–438.

Camp, V.E., Ross, M.E., 2004. Mantle dynamics and genesis of mafic magmatism in the intermontane Pacific Northwest. Journal of Geophysical Research 109 (B08204) 14 pp. doi:10.1029/2003JB002838.

Camp, V.E., Hanan, B.B., 2008. A plume-triggered delamination origin for the Columbia River Basalt Group. Geosphere 4, 480–495.

Campbell, I.H., 2007. Testing the plume theory. Chemical Geology 241, 153–176.

Campbell, I.H., Kerr, A.C. (Eds.), 2007. The Great Plume Debate: Chemical Geology (Issues 3–4), vol. 241, pp. 149–374.

Carlson, R.W., Hart, W.K., 1987. Crustal genesis of the Oregon Plateau. Journal of Geophysical Research 92, 6,191–6,206.

Carlson, R.W., Hart, W.K., 1988. Flood basalt volcanism in the northwestern United States. In: MacDougall, J.D. (Ed.), Continental Flood Basalts. Kluwer Academic Publishers, Dordrecht, The Netherlands, pp. 35–61.

Christiansen, R.L., 2001. The Quaternary and Pliocene Yellowstone Plateau volcanic field of Wyoming, Idaho, and Montana. U.S. Geological Survey Professional Paper 729 G 145 pp.

Christiansen, R.L., Yeats, R.S., 1992. Post-Laramide geology of the U.S. Cordilleran region. In: Burchfiel, B.C., Lipman, P.W., Zoback, M.L. (Eds.), The Cordilleran orogen: Conterminous U.S. Geological Society of America: Geology of North America, vol. G-3, pp. 261–406.

Christiansen, R.L., Foulger, G.R., Evans, J.R., 2002. Upper mantle origin of the Yellowstone hotspot. Geological Society of America Bulletin 114, 1245–1256.

Coble, M.A., Mahood, G.A., 2008. New geologic evidence for additional 16.5–15.5 Ma silicic calderas in northwest Nevada related to initial impingement of the Yellowstone hotspot. Collapse Calderas Workshop: IOP Conference Series, Earth and Environmental Sciences, vol. 3. doi:10.1088/1755-1307/3/1/12002.

Colgan, J.P., Dumitru, T.A., Miller, E.L., 2004. Diachroneity of Basin and Range extension and Yellowstone hotspot volcanism in northwestern Nevada. Geology 32, 121–124.

Colgan, J.P., Dumitru, T.A., Reiners, P.W., Wooden, J.L., Miller, E.L., 2006. Cenozoic tectonic evolution of the Basin and Range province in northwestern Nevada. American Journal of Science 306, 616–654. doi:10.2475/08.2006.02.

Colgan, J.P., John, D.A., Henry, C.C., Fleck, R.J., 2008. Large-magnitude Miocene extension of the Eocene Caetano caldera, Shoshone and Toiyabe Ranges, Nevada. Geosphere 4, 107–130. doi:10.1130/GES00115.1.

Courtillot, V., Davaille, A.B.J., Stock, J., 2003. Three distinct types of hotspots in the Earth's mantle. Earth and Planetary Science Letters 205, 295–308.

Craig, H., 1997. Helium isotope ratios in Yellowstone Park and along the Snake River Plain: Backtracking the Yellowstone hotspot. EOS, Transactions, American Geophysical Union, Abstracts: Fall Meeting, vol. 78: F801 (V32G-2).

Crough, S.T., 1978. Thermal origin of mid-plate hot-spot swells. Geophysical Journal of the Royal Astronomical Society 55, 451–469.

Crough, S.T., 1983. Hot spot swells. Annual reviews of the Earth and Planetary Sciences 11, 165–193.

Cummings, M.L., Evan, J.G., Ferns, M.L., Lees, K.R., 2000. Stratigraphic and structural evolution of the middle Miocene synvolcanic Oregon–Idaho graben. Geological Society of America Bulletin 112, 668–682.

Davis, G.F., 1999. Dynamic Earth, Plates, Plumes, and Mantle Convection. Cambridge University Press, Cambridge, U.K. 458 pp.

Davis, O.K., Ellis, B., Link, P., Wood, S., Shervais, J.W., 2006. Neogene palynology of the Snake River Plain: climate change and volcanic effects. EOS Transactions of AGU, Abstracts: Fall Meeting, vol. 57, V43D-08.

Dickinson, W.R., 1997. Tectonic implications of Cenozoic volcanism in coastal California. Geological Society of America Bulletin 109, 936–954.

Dickinson, W.R., 2006. Geotectonic evolution of the Great Basin. Geosphere 2, 353–368.

Dickinson, W.R., Snyder, W.S., 1979. Geometry of subducted slabs related to the San Andreas Transform. Journal of Geology 87, 609–627.

Dodson, A., Kennedy, B.M., DePaolo, D.J., 1997. Helium and neon isotopes in the Imnaha Basalt, Columbia River Basalt Group: evidence for a Yellowstone plume source. Earth and Planetary Science Letters 150, 443–451.

Draper, D.S., 1991. Late Cenozoic bimodal magmatism in the northern Basin and Range Province of Southeastern Oregon. Journal of Volcanology and Geothermal Research 47, 299–328.
Elison, M.W., Speed, R.C., Kistler, R.W., 1990. Geologic and isotopic constraints on the crustal structure of the northern Great Basin. Geological Society of America Bulletin 102, 1,077–1,092.
Ernst, E.E., Buchan, K.L., 2001a. The use of mafic dike swarms in identifying and locating mantle plumes. In: Ernst, R.E., Buchan, K.L. (Eds.), Mantle Plumes: Their Identification Through Time: Geological Society of America Special Paper, vol. 352, pp. 247–265.
Ernst, R.E., Buchan, K.L. (Eds.), 2001b. Mantle Plumes: Their Identification through Time: Geological Society of America Special Paper, vol. 352. 593 pp.
Fee, D., Dueker, K., 2004. Mantle transition zone topography and structure beneath the Yellowstone hotspot. Geophysical Research Letters 31 (L18603). doi:10.1029/2004GL020636.
Fosdick, J.C., Colgan, J.P., 2008. Miocene extension in the East range, Nevada: a two-stage history of normal faulting in the northern Basin and Range. Geological Society of America Bulletin 120, 1198–1213. doi:10.1130/B26201.1.
Foulger, G.R., Natland, J.H., 2003. Is "hotspot" volcanism a consequence of plate tectonics? Science 300, 921–922. doi:10.1026/science.1083376.
Foulger, G.R., Natland, J.H., Anderson, D.L., 2004. Plume IV: Beyond the plume hypothesis—tests of the plume paradigm and alternatives. GSA Today 14, 26–28.
Fritz, W.J., Sears, J.W., 1993. Tectonics of the Yellowstone hotspot wake in southwestern Montana. Geology 21, 427–430.
Fritz, W.J., Sears, J.W., McDowell, R.J., Wampler, J.M., 2007. Cenozoic volcanic rocks of Southwestern Montana. In: Thomas, R.C., Gibson, R.I. (Eds.), Introduction to the Geology of the Dillon Area: Northwest Geology, vol. 36, pp. 91–110.
Garrison, N.J., Busby, C.J., Gans, P., Wagner, D., 2008. A mantle plume beneath California? The Mid-Miocene Lovejoy flood basalt, northern California. In: Wright, J., Shervais, J. (Eds.), Ophiolites, Arcs, and Batholiths: Geological Society of America Special Paper, vol. 438. 22pp.
Geist, D., Richards, M., 1993. Origin of the Columbia Plateau and Snake River Plain: deflection of the Yellowstone plume. Geology 21, 789–792.
Glen, J.M.G., Ponce, D.A., 2002. Large-scale fractures related to inception of the Yellowstone hotspot. Geology 30, 647–650.
Gonnermann, H.L., Mukhopadhyay, S., 2007. Non-equilibrium degassing and primordial source for helium in ocean-island volcanism. Nature 449, 1,037–1,040.
Graham, D.W., Reid, M.R., Jordan, B.T., Grunder, A.L., Leeman, W.P., Lupton, J.E., 2007. Mantle source provinces beneath the Pacific northwest revealed by helium isotope variations in basaltic lavas. Geological Society of America Abstracts with Programs 39 (6), 455, 169–1.
Graham, D.W., Reid, M.R.., Jordan, B.T., Grunder, A.L., Leeman, W.P., Lupton, J.E, 2009. Mantle source provinces beneath the northwestern USA delimited by helium isotopes in young basalts. In: Morgan, L.A., Cathey, H.E., Pierce, K.L. (Eds.), Track of the Yellowstone Hotspot. Journal of Volcanology and Geothermal Research, 188, pp. 128–140.
Gripp, A.E., Gordon, R.G., 1990. Current plate velocities relative to hot-spots incorporating the NUVEL-1 global plate motion model. Geophysical Research Letters 17, 1109–1112.
Gripp, A.E., Gordon, R.G., 2002. Young tracks of hotspots and current plate velocities. Geophysical Journal International 150, 321–361.
Hales, T.C., Abt, D.L., Humphreys, E.D., Roering, J.J., 2005. A lithospheric instability origin for Columbia River flood basalts and Wallowa Mountains uplift in northeast Oregon. Nature 438, 842–845.
Hamilton, W.B., 1989. Crustal geologic processes of the United States. In: Pakiser, L.C., Mooney, W.D. (Eds.), Geophysical Framework of the Continental Unites States: Geological Society of America Memoir, vol. 172, pp. 743–781.
Hamilton, W.B., 1999. Middle and late Cenozoic tectonics and topographic changes in the western United States. Geological Society of America Abstracts with Programs 31 (7), 443.
Hamilton, W.B., 2003. An alternative earth. GSA Today 4–12 November.
Hemphill-Haley, M.A., Sawyer, T.L., Knuepfer, P.L.K., Forman, S.L., Wong, I.G., 2000. Timing of faulting events from thermoluminescence dating of scarp-related deposits, Lemhi fault, southeastern Idaho. In: Noller, J.S., Sowers, J.M., Lettis, W.R. (Eds.), Quaternary Geochronology, Methods and Applications: Washington, D.C. AGU Reference Shelf, vol. 4, pp. 541–548.
Hershler, R., Liu, H.P., Gustafson, D.L., 2008. A second species of Pyrgulopsis (Hydrobiidae) from the Missouri River Basin, with molecular evidence supporting faunal origin through Pliocene stream capture across the northern Continental Divide. Journal of Molluscan Studies 74, 403–413.
Hill, R.I., Campbell, G.F., Davies, G.F., Griffiths, R.W., 1992. Mantle plumes and continental tectonics. Science 256, 186–193.
Hirose, K., 2002. Phase transitions in pyrolitic mantle around 670-km depth: implications for upwelling of plumes from the lower mantle. Journal of Geophysical Research 107 (B4). doi:10.1029/2001JB000597.
Hittelman, A.M., Dater, D.T., Buhmann, R.W., Racey, S.D., 1994. Gravity-1994 edition (CD-ROM); National Geophysical data Center, Boulder CO, flier SE-1703.
Hodges, M.K.V., 2006, Tertiary stratigraphy of the Idaho Medicine Lodge Valley, Clark County, Idaho: MS thesis, Idaho State University, Pocatello, Idaho, 163 p.
Hodges, M.K.V., Link, P.K., Fanning, C.M., 2009. The Pliocene Lost River found to west: Detrital zircon evidence of drainage disruption along a subsiding hotspot track. In: Morgan, L.A., Cathey, H.E., Pierce, K.L. (Eds.), Track of the Yellowstone Hotspot. Journal of Volcanology and Geothermal Research, 188, pp. 237–249.
Hooper, P.R., 1990. The timing of crustal extension and the eruption of continental flood basalts. Nature 345, 246–249.
Hooper, P.R., Camp, V., Reidel, S., Ross, M., 2007. The origin of the Columbia River flood basalt province: plume versus nonplume models. In: Foulger, G.R., Jurdy, D.M. (Eds.), Plates, Plumes, and Planetary Processes: Geological Society of America Special Paper, vol. 430, pp. 635–668.
Horton, T.W., Chamberlain, C.P., 2006. Stable isotopic evidence for Neogene surface downdrop in the central Basin and Range province. Geological Society of America Bulletin 118, 475–490.
Horton, T.W., Sjostrom, D.J., Abruzzese, M.J., Poage, M.A., Waldbauer, J.R., Hren, M., Wooden, J., Chamberlain, C.P., 2004. Spatial and temporal variation of Cenozoic surface elevation in the Great Basin and Sierra Nevada. American Journal of Science 304, 862–888.
Hughes, S.S., McCurry, M.i.c.h.a.e.l., 2002. Bulk major and trace element evidence for a time–space evolution of Snake River Plain rhyolites, Idaho. In: Bonnichsen, Bill, White, C.M., McCurry, Micheal (Eds.), Tectonic and Magmatic Evolution of the Snake River Plain Volcanic Province: Idaho Geological Survey Bulletin, vol. 30, pp. 161–171.
Humphreys, E.D., Coblentz, D.D., 2007. North American dynamics and western U.S. Tectonics. Reviews of Geophysics 43. 30 pp.
Humphreys, E.D., Dueker, K.G., Schutt, D.L., Smith, R.B., 2000. Beneath Yellowstone: evaluating plume and nonplume models using teleseismic images of the upper mantle. GSA Today 10, 1–6.
Ito, G., Mahoney, J.J., 2006. Melting a high $^{3}He/^{4}He$ source in a heterogeneous mantle. Geochemistry, Geophysics, Geosystems 7. doi:10.1029/2005GC001158.
Janecke, S.U., 2007. Cenozoic extensional processes and tectonics in the northern Rocky Mountains: Southwest Montana and eastern Idaho. Northwest Geology 36, 111–132.
Janecke, S.U., Blankenau, J.J., VanDenburg, C.J., Van Gosen, B.S., 2001. Normal faults and extensional folds of southwestern Montana and eastern Idaho: Geometry, relative ages, and tectonic significance. U.S. Geological Survey Miscellaneous Field Studies Map 2362, scale 1:100,000.
Jaworowski, C., 1994. Geologic implications of Quaternary tephra localities in the western Wind River Basin, Wyoming. In: Keefer, W.R., Metzger, S.J., Godwin, L.H. (Eds.), Oil and Gas and Other Resources of the Wind River Basin, Wyoming. Wyoming Geological Association Special Symposium, pp. 191–205.
John, D.A., 2001. Miocene and early Pliocene epithermal gold–silver deposits in the northern Great Basin, western United States: characteristics, distribution, and relationship to magmatism. Economic Geology 96, 1827–1853.
John, D.A., Wallace, A.R., 2000. Epithermal gold–silver mineral deposits related to the northern Nevada rift: Geological Society of Nevada, Geology and Ore Deposits 2000. The Great Basin and Beyond Symposium, May 15–18, 2000, Reno-Sparks, Nevada, Proceedings, pp. 155–175.
John, D.A., Wallace, A.R., Ponce, D.A., Fleck, R.B., Conrad, J.E., 2000. New perspectives on the geology and origin of the northern Nevada rift. In: Cluer, J.K., Price, J.G., Struhsacker, E.M., Hardyman, R.F., Morris, D.L. (Eds.), Geology and Ore deposits 2000: The Great Basin and Beyond. Geological Society of Nevada Symposium Proceedings, May 15–18, pp. 127–154.
Jordan, T.H., 1979. Mineralogies, densities, and seismic velocities of garnet lherzolites and their geophysical implications. In: Boyd, F.R. (Ed.), The Mantle Sample: Inclusions in kimberlites and other volcanics. Proceedings of the 2nd International Kimberlite Conference, vol. 2. American Geophysical Union, Washington, D.C., pp. 1–14.
Jordan, B.J., Grunder, A.L., Duncan, R., Deino, A., 2004. Geochronology of age-progressive volcanism of the Oregon High Lava Plains: implications for the plume interpretation of Yellowstone. Journal of Geophysical Research 109 (B10202). doi:10.1029/2003JB002726.
Kamenov, G.D., Saunders, J.A., Hames, W.E., Unger, D.L., 2007. Mafic magmas as sources for gold in middle Miocene epithermal deposits of the northern Great Basin, United States: evidence from *Pb* isotope compositions of native gold. Economic Geology 102, 1,191–1,195.
Kellogg, D.S., Lanphere, M., 1988. New potassium–argon ages, geochemistry, and tectonic setting of upper Cenozoic volcanic rocks near Blackfoot, Idaho. U.S. Geological Survey Bulletin 1086, 19 pp.
Kennedy, B.M., Reynolds, J.H., Smith, S.P., Truesdell, A.H., 1987. Helium isotopes: lower Geyser Basin, Yellowstone National Park. Journal of Geophysical Research 92, 12,477–12,489.
Ketner, K.B., Keefer, W.R., Fisher, F.S., Smith, D.L., Raabe, R.G., 1966. Mineral resources of the stratified primitive area, Wyoming. U.S. Geological Survey Bulletin 1230-E. 56 pp.
Kreemer, C., Hammond, W.C., 2007. Geodetic constraints on areal changes in the Pacific–North America plate boundary zone: what controls Basin and Range extension? Geology 35, 943–946.
Kuntz, M.A., Covington, H.R., Schorr, L.J., 1992. An overview of basaltic volcanism of the eastern Snake River Plain, Idaho. In: Link, P.K., Kuntz, M.A., Platt, L.B. (Eds.), Regional Geology of Eastern Idaho and Western Wyoming: Geological Society of America Memoir, vol. 179, pp. 227–267.
Kurz, M.D., Jenkins, W.J., Hart, S.R., 1982. Helium isotopic systematics of ocean islands and mantle heterogeneity. Nature 297, 43–47.
Lageson, D.R., Stickney, M.C., 2000. Seismotectonics of northwest Montana, USA. In: Schalla, R.A., Johnson, E.H. (Eds.), Montana/Alberta Thrust Belt and Adjacent Foreland. 50th Anniversary Symposium, vol. 1. Montana Geological Society, pp. 109–126.
Lay, T., ed. 2009. Seismological Grand Challenges in Understanding Earth's Dynamic Systems. Report to the National Science Foundation, IRIS Consortium, 76 pp. Yellowstone plume tomography diagram on p. 46, courtesy of Richard Allen.
Lay, T., Hernlund, J., Buffett, B.A., 2008. Core–mantle boundary heat flow. Nature Geoscience 1, 25–32.
Leeman, W.P., 2005. Origin of Snake River Plain–Yellowstone (SRPY) basaltic magmas: lithospheric vs. asthenospheric contributions. Geological Society of America, Abstracts with Programs 7, 37, 201.
Link, P.K., Christie-Blick, N., Stewart, J.H., Miller, J.M.G., Devlin, W.J., Levy, M., 1993. Late Proterozoic strata of the United States Cordillera. In: Reed, J.C., Bickford, M.E., Houston, R.S., Link, P.K., Rankin, D.W., Sims, P.K., Van Schmus, W.R. (Eds.), Precambrian: Conterminous U.S. Geological Society of America: The Geology of North America, Boulder, vol. C-2, pp. 536–558.

Link, P.K., Reading, R.W., Godfrey, A.E., Prevedel, D., 1999. The track of the Yellowstone hot spot. GIS Center for Excellence, DEM Models, version 7–99. USDA Forest Service, Ogden, Utah.
Link, P.K., McDonald, H.G., Fanning, C.M., Godfrey, A.E., 2002. Detrital Zircon Evidence for Pleistocene Drainage Reversal at Hagerman Fossil Beds National Monument, Central Snake River Plain, Idaho. In: Bonnichsen, Bill, White, C.M., McCurry, Micheal (Eds.), Tectonic and Magmatic Evolution of the Snake River Plain Volcanic Province: Idaho Geological Survey Bulletin, vol. 30, pp. 105–119.
Link, P.K., Fanning, C.M., Beranek, L.P., 2005. Reliability and longitudinal change of detrital-zircon age spectra in the Snake River system, Idaho and Wyoming: an example of reproducing the bumpy barcode. Sedimentary Geology 182, 101–142.
Lipman, P.W., 1992. Magmatism in the Cordilleran United States; progress and problems. In: Burchfiel, B.C., Lipman, P.W., Zoback, M.L. (Eds.), The Cordilleran Orogen: Conterminous U.S. The Geology of North America, vol. G-3. Geological Society of America, pp. 481–514.
Long, S.P., Link, P.K., Janecke, S.U., Perkins, M.E., Fanning, C.M., 2006. Multiple phases of Tertiary extension and synextensional deposition of the Miocene–Pliocene Salt Lake Formation in an evolving supradetachment basin, Malad Range, southeast Idaho, U.S.A. Rocky Mountain Geology 41, 1–27.
Lowry, A.R., Ribe, N.M., Smith, R.B., 2000. Dynamic elevation of the Cordillera, western United States. Journal of Geophysical Research 105, 23,371–23,390.
MacLeod, N.S., Walker, G.W., McKee, E.H., 1976. Geothermal significance of eastward increase in age of upper Cenozoic rhyolitic domes in southeastern Oregon: proceedings of the Second United Nations Symposium on the Development and Use of Geothermal Resources, Washington, D.C. U.S. Government Printing Office 1, 456–474.
Manley, C.R., McIntosh, W.C., 2002. The Juniper Mountain volcanic center, Owyhee County, southwestern Idaho: age relations and physical volcanology. In: Bonnichsen, Bill, White, C.M., McCurry, Micheal (Eds.), Tectonic and Magmatic Evolution of the Snake River Plain Volcanic Province: Idaho Geological Survey Bulletin, vol. 30, pp. 205–227.
Malde, H.E., 1991. Quaternary geology and structural history of the Snake River Plain, Idaho and Oregon. In: Morrison, R.B. (Ed.), Quaternary Nonglacial History of the Conterminous U.S. The Geology of North America, vol. K-2, Ch. 4. Geological Society of America, pp. 251–282.
McNamara, A.K., van Keken, P.E., 2000. Cooling of the Earth: a parameterized convection study of whole versus layered models. Geochemistry, Geophysics, Geosystems 1 (11), 1027. doi:10,1029/2000GC00045.
McQuarrie, N., Rodgers, D.W., 1998. Subsidence of a volcanic basin by flexure and lower crustal flow: the eastern Snake river Plain, Idaho. Tectonics 17, 203–220.
Molnar, P., England, P., 1990a. Surface uplift, uplift of rocks, and exhumation of rocks. Geology 18, 1,173–1,177.
Molnar, P., England, P., 1990b. Late Cenozoic uplift of mountain ranges and global climate change: chicken or egg? Nature 346, 29–34.
Montelli, R., Nolet, G., Dahlen, F.A., Masters, G., 2006. A catalog of deep mantle plumes: New results from finite frequency tomography. Geochemistry, Geophysics, Geosystems 7. doi:10.1029/GC001248.
Mooney, W.D., Weaver, C.S., 1989. Regional crustal structure and tectonics of the Pacific coastal states: California, Oregon, and Washington. In: Pakiser, L.C., Mooney, W.D. (Eds.), Geophysical Framework of the Continental United States: Geological Society of America Memoir, vol. 172, pp. 129–161.
Morgan, W.J., 1972. Plate motions and deep mantle convection. Geological Society of America Memoir 132, 7–22.
Morgan, P., Gosnold, W.D., 1989. Heat flow and thermal regimes of the continental United States. In: Pakiser, L.C., Mooney, W.D. (Eds.), Geophysical Framework of the Continental United States: Geological Society of America Memoir, vol. 172, pp. 493–522.
Morgan, L.A., McIntosh, W.C., 2005. Timing and development of the Heise volcanic field, Snake River Plain, Idaho western USA. Geological Society of America Bulletin 117, 288–301.
Morgan, J.P., Morgan, W.J., Price, E., 1995. Hotspot melting generates both hotspot volcanism and hotspot swell? Journal of Geophysical Research B5, 100, 8,045–8,062.
Morgan, L.A., McIntosh, W.C., Pierce, K.L., 1997. Inferences for changes in plume dynamics from stratigraphic framework studies of ignimbrites, central Snake River Plain, Idaho. Geological Society of America, Abstracts with Programs 29, A299.
Morgan, L.A., Pierce, K.L., Shanks, W.C. Pat., 2008. Track of the Yellowstone hotspot: Young and ongoing geologic processes from the Snake River Plain to the Yellowstone Plateau and Tetons. In: Raynolds, R.G. (Ed.), Roaming the Rocky Mountains and Environs: Geological Field Trips: Geological Society of America Field Guide, vol. 10, pp. 139–173.
Mueller, K.J., Cerveny, P.K., Perkins, M.E., Snee, L.W., 1999. Chronology of polyphase extension in the Windermere Hills, northeast Nevada. Geological Society of America Bulletin 111, 11–27.
Naeser, C.W., Izett, G.A., Obradovich, J.D., 1980. Fission-track and K–Ar ages of natural glasses. U.S. Geological Survey Bulletin 1489. 31 pp.
Olig, S.S., Gorton, A.E., Bott, J.D., Wong, I.G., Knuepfer, P.K.L., Forman, S.L., Smith, R.P., Simpson, D., 1995. Paleoseismic investigation of the southern Lost River fault, Idaho. Idaho National Engineering Laboratory Report INEL-95/508, prepared by Woodward-Clyde Federal Services for Lockheed Martin Idaho Technologies.
Olig, S.S., Gorton, A.E., Smith, R.P., Forman, S.L., 1997. Additional geological investigations of the southern Lost River fault and northern Arco rift zone, Idaho, Unpublished report prepared by Woodward-Clyde Federal Services for Lockheed Martin Technologies Company, Project No. SK9654.
Pakiser, L.C., 1989. Geophysics of the Intermontane system. In: Pakiser, L.C., Mooney, W.D. (Eds.), Geophysical Framework of the Continental United States: Geological Society of America Memoir, vol. 172, pp. 235–247.
Parsons, T., 1995. The Basin and Range Province. In: Olsen, K.H. (Ed.), Continental Rifts: Evolution, Structure, Tectonics. Developments in Geotectonics, vol. 25. Elsevier, Amsterdam, pp. 277–324.
Parsons, T., Thompson, G.A., Sleep, N.H., 1994. Mantle plume influence on the Neogene uplift and extension of the U.S. western Cordillera? Geology 22, 83–86.
Parsons, T., Thompson, G.A., Smith, R.P., 1998. More than one way to stretch: a tectonic model for extension along the plume track of the Yellowstone hotspot and adjacent Basin and Range Province. Tectonics 17, 221–234.
Perkins, M.E., Nash, B.P., 2002. Explosive silicic volcanism of the Yellowstone hotspot: the ash fall tuff record. Geologic Society of America Bulletin 114, 367–381.
Perkins, M.E., Brown, F.H., Nash, W.P., McIntosh, W., Williams, S.K., 1998. Sequence, age, and source of silicic fallout tuffs in middle to late Miocene basins of the Basin and Range province. Geological Society of America Bulletin 110, 344–360.
Pierce, K.L., Morgan, L.A., 1990. The track of the Yellowstone hot spot: volcanism, faulting, and uplift. U.S. Geological Survey Open-File Report 90-415. 49 pp.
Pierce, K.L., Good, J.D., 1992. Field guide to the Quaternary geology of Jackson Hole, Wyoming. U.S. Geological Survey Open-File Report 92-504. 49 pp.
Pierce, K.L., Morgan, L.A., 1992. The track of the Yellowstone hot spot: volcanism, faulting, and uplift. In: Link, P.K., Kuntz, M.A., Platt, L.B. (Eds.), Regional Geology of Eastern Idaho and Western Wyoming: Geological Society of America Memoir, vol. 179, pp. 1–53.
Pierce, K.L., Morgan, L.A., 2005. Asymmetrical features across the Yellowstone hotspot track and the northwest inclination of the Yellowstone plume. Geological Society of America Abstracts with Programs 37 (7), 127.
Pierce, K.L., Morgan, L.A., Saltus, R.W., 2002. Yellowstone plume head: postulated tectonic relations to the Vancouver slab, continental boundaries, and climate. In: Bonnichsen, Bill, White, C.M., McCurry, Micheal (Eds.), Tectonic and Magmatic Evolution of the Snake River Plain Volcanic Province: Idaho Geological Survey Bulletin, vol. 30, pp. 5–33.
Pierce, K.L., Morgan, L.A., Saltus, R.W., 2007. The Yellowstone hotspot track—integrated parameters favor model of a deep-seated plume head followed by a plume tail. Geological Society of America Abstracts with Programs 39 (6), 291.
Putirka, Keith, 2008. Excess temperatures at ocean islands: implications for mantle layering and convection. Geology 36, 283–286. doi:10.1130/G24615A.1.
Richards, M.A., Duncan, R.A., Courtillot, V.E., 1989. Flood basalts and hot spot tracks: plume heads and tails. Science 246, 103–107.
Rodgers, D.W., Hackett, W.R., Ore, H.T., 1990. Extension of the Yellowstone Plateau, eastern Snake River Plain, and Owyhee Plateau. Geology 18, 1,138–1,141.
Rodgers, D.W., Ore, H.T., Bobo, R.T., McQuarrie, N., Zentner, N., 2002. Extension and subsidence of the Eastern Snake River Plain, Idaho. In: Bonnichsen, B., White, C.M., McCurry, Micheal (Eds.), Tectonic and Magmatic Evolution of the Snake River Plain Volcanic Province: Idaho Geological Survey Bulletin, vol. 30, pp. 121–155.
Roth, J.B., Fouch, M.J., James, D.E., Carlson, R.W., 2008. Three dimensional seismic velocity structure of the northwestern United States. Geophysical Research Letters 35 (L15304,). doi:10.1029/2008GLO34669.
Rowley, P.W., 2001. The Cenozoic evolution of the Great Basin area, U.S.A.—new interpretations based on regional geologic mapping. In: Erskine, M.C. (Ed.), The Geologic Transition, High Plateaus to Great Basin — A Symposium and Field Guide (The Mackin Volume): Utah Geological Association Publication, vol. 30, pp. 169–188.
Saltus, R.W., Thompson, G.A., 1995. Why is it downhill from Tonopah to Las Vegas?: a case for a mantle plume support of the high northern Basin and Range. Tectonics 14, 1,235–1,244.
Saunders, A.D., Jones, S.M., Morgan, L.A., Pierce, K.L., Widdowson, M., Xu, Y.G., 2007. Regional uplift associated with continental large igneous provinces: the roles of mantle plumes and the lithosphere. Chemical Geology 241, 282–318. doi:10.1016/j.chemgeo.2007.01.017.
Schubert, G., Turcotte, D.L., Olson, Peter, 2001. Mantle Convection in the Earth and Planets. Cambridge University Press, Cambridge, U.K. 940 pp.
Schutt, D.L., Dueker, K., 2008. Temperature of the plume layer beneath the Yellowstone hotspot. Geology 36, 623–626. doi:10.1130/G24809A.1.
Schutt, D.L., Dueker, K., Yuan, H., 2008. Crust and upper mantle velocity structure of the Yellowstone hotspot and surroundings. Journal of Geophysical Research 113 (B03310). doi:10.1029/2007JB005109.
Sears, J.W., Fritz, W.J., 1998. Cenozoic tilt-domains in southwest Montana: interference among three generations of extensional fault systems. In: Faulds, J.E., Stewart, J.H. (Eds.), Accommodation Zones and Transfer Zones: The Regional Segmentation of the Basin and Range Province: Geological Society of America Special Paper, vol. 323, pp. 241–248.
Sears, J.W., Thomas, R.C., 2007. Extraordinary middle Miocene crustal disturbance in southwest Montana: birth record of the Yellowstone hot spot? In: Thomas, R.C., Gibson, R.I. (Eds.), Introduction to the Geology of the Dillon area: Northwest Geology: Dillon Field Conference, vol. 36, pp. 133–142.
Sears, J.W., Hendrix, M.S., Thomas, R.C., Fritz, W.J., 2009. Stratigraphic record of the Yellowstone hotspot track, Neogene Sixmile Creek Formation grabens, southwest Montana. In: Morgan, L.A., Cathey, H.E., Pierce, K.L. (Eds.), 2009. Track of the Yellowstone Hotspot. Journal of Volcanology and Geothermal Research, 188, pp. 250–259.
Şengör, A.M.C., 2001. Elevation as indicator of mantle–plume activity. In: Ernst, R.E., Buchan, K.L. (Eds.), Mantle Plumes: Their Identification Through Time: Geological Society of America Special Paper, vol. 352, pp. 183–225.
Severinghaus, J., Atwater, T., 1990. Cenozoic geometry and thermal state of the subducting slabs beneath western North America. In: Wernicke, B.P. (Ed.), Basin and Range Extensional Tectonics Near the Latitude of Las Vegas, Nevada: Geological Society of America Memoir, vol. 176, pp. 1–22.
Sharp, W.P., Ludwig, K.R., Chadwick, O.A., Amundson, Ron, Glaser, L.L., 2003. Dating fluvial terraces by 230^{Th}/U on pedogenic carbonate, Wind River Basin, Wyoming. Quaternary Research 59, 139–150.
Shervais, J.W., Hanan, B.B., 2008. Lithospheric topography, tilted plumes, and the track of the Snake River–Yellowstone hot spot. Tectonics 27 (TC5004). doi:10/1029/2007/TC002181 17 pp.

Sleep, N.H., 1990. Hotspots and mantle plumes: some phenomenology. Journal of Geophysical Research B5, 95, 6,715–6,736.
Sleep, N.H., 1997. Lateral flow and ponding of starting plume material. Journal of Geophysical Research B5 102, 10,001–10,012.
Sleep, N.H., 2006. Mantle plumes from top to bottom. Earth Science Reviews 77, 231–271.
Smedes, H.W., M'Gonigle, J.W., Prostka, H., 1989. Geologic map of the Two Ocean Pass quadrangle, Yellowstone National Park and vicinity, Wyoming. U.S. Geological Survey Geologic Quadrangle Map, GQ-1667, scale 1:62,500.
Smith, G.R., 1981. Late Cenozoic freshwater fishes of North America. Annual Reviews of Ecological Systems 12, 163–193.
Smith, A.D., 1992. Back-arc convection model for Columbia River basalt genesis. Tectonophysics 207, 269–285.
Smith, R.B., Braile, L.W., 1993. Topographic signature, space–time evolution, and physical properties of the Yellowstone–Snake River Plain volcanic system: the Yellowstone hotspot. In: Snoke, A.W., Steidtmann, J.R., Roberts, S.M. (Eds.), Geology of Wyoming: Geological Survey of Wyoming Memoir, vol. 5, pp. 694–754.
Smith, G.R., Patterson, W.P., 1994. Mio-Pliocene seasonality on the Snake River Plain: comparison of faunal and oxygen isotopic evidence. Palaeogeography, Palaeoclimatology, Palaeoecology 107, 291–302.
Smith, R.B., Shuey, R.T., Freidline, R.O., Otis, R.M., Alley, L.B., 1974. Yellowstone hotspot: new magnetic and seismic evidence. Geology 2, 451–455.
Smith, R.B., Farrell, J., Jordan, M., Puskas, C., Waite, G.P., 2007. Seismic and GPS constraints on dynamics and kinematics of the Yellowstone volcanic field. Eos Transactions of the American Geophysical Union: Fall Meeting Supplement, Abstract V51F-02, vol. 88(52).
Smith, R.B., Jordan, M., Steinberger, B., Puskas, C.M., Farrell, J., Waite, G.P., Husen, S., Chang, W.L., O'Connell, R.O., 2009. Geodynamics of the Yellowstone Hotspot and Mantle plume: Seismic and GPS imaging, kinematics, and mantle flow. In: Morgan, L.A., Cathey, H.E., Pierce, K.L. (Eds.), Track of the Yellowstone Hotspot. Journal of Volcanology and Geothermal Research, 188, pp. 26–56.
Steinberger, B., 2000. Plumes in a convecting mantle: models and observations for individual hotspots. Journal of Geophysical Research 105, 11,127–11,152.
Streck, Martin J., Grunder, Anita L., 2008. Phenocryst-poor rhyolites of bimodal, tholeiitic provinces: the Rattlesnake Tuff and implications for mush extraction models. Bulletin Volcanology 70, 385–401.
Stroup, C.N., Link, P.K., Janecke, S.U., Fanning, C.M., Yaxley, G.M., Beranek, L.P., in press. Eocene to Oligocene provenance and drainage in extensional basins of southwest Montana and east-central Idaho: Evidence from detrital zircon populations in the Renova Formation and equivalent strata. In Spencer, J.E., Titley, S.R., (Eds.), Circum-Pacific Tectonics, Geologic Evolution, and Ore Deposits: Tucson, Arizona Geological Society, Digest 22, p. xx–xxx.
Stroup, C.N., Sears, J.W., Link, P.K., 2008a. Idaho sources for detrital zircons in late Miocene Sixmile Creek Formation, SW Montana. Geological Society of America Abstracts with Programs 40 (1), 78.
Stroup, C.N., Link, P.K., Fanning, C.M., 2008b. Provenance of late Miocene fluvial strata of the Sixmile Creek Formation, southwest Montana: evidence from detrital zircon. Northwest Geology 37, 69–84.
Suppe, J., Powell, C., Berry, R., 1975. Regional topography, seismicity, Quaternary volcanism, and the present-day tectonics of the western United States. American Journal of Science 275A, 397–436.
Takahahshi, E., Katsuji, N., Wright, T.L., 1998. Origin of the Columbia River basalts: melting model of a heterogeneous plume head. Earth and Planetary Science Letters 162 (1–4), 63–80.
Taubeneck, W.H., 1970. Dikes of Columbia River basalt in northeastern Oregon, western Idaho, and south-eastern Washington. In: Gilmore, E.H., Strandling, D. (Eds.), Proceedings of the Second Columbia River Basalt Symposium. Eastern Washington State college, Cheney, pp. 73–96.
Tauzin, B., Debayle, E., Wittlinger, G., 2008. The mantle transition zone as seen by global *Pds* phases: no clear evidence for a thin transition zone beneath hotspots. Journal of Geophysical Research 113. doi:10.1029/2007JB005364. 17 pp.
Taylor, D.W., Bright, R.C., 1987. Drainage history of the Bonneville Basin, in Cenozoic Geology of Western Utah. Utah Geological Association Publication 16, 239–256.
Thompson, G.A., 1998. Deep mantle plumes and geoscience vision. GSA Today 8 (4), 7–25.
Thompson, R.N., Gibson, S.A., 1991. Subcontinental mantle plumes, hotspots, and pre-existing thinspots. Journal of the Geological Society 148, 973–977.
Tolan, T.L., Reidel, S.P., Beeson, M.H., Anderson, J.L., Fecht, K.R., Swanson, D.A., 1989. Revisions of the extent and volume of the Columbia River Basalt Group. In: Reidel, S.P., Hooper, P.R. (Eds.), Volcanism and Tectonism in the Columbia River Flood-Basalt Province: Geological Society of America Special Paper, vol. 239, pp. 1–20.
Wagner, D.L., Saucedo, G.J., Grose, T.L.T., 2000. Tertiary volcanic rocks of the Blairsden area, northern Sierra Nevada, California. In: Brooks, R.R., Dida, L.T. (Eds.), Field Guide to the Geology and Tectonics of the Northern Sierra Nevada: National Association of Geoscience Teachers, Far West Section, Fall conference: California Division of Mines and Geology Special Publication, vol. 122, pp. 155–172.
Waite, G.P., Smith, R.B., 2002. Seismic evidence for fluid migration accompanying subsidence of the Yellowstone caldera. Journal of Geophysical Research 107 (B9), 2177. doi:10.1029/2001JB000586.
Waite, G.P., Smith, R.L., Allen, R.L., 2006. *VP* and *VS* structure of the Yellowstone Hotspot from teleseismic tomography: evidence for an upper mantle plume. Journal of Geophysical Research 111 (B04303). doi:10.1029/2005JB003867. 21 pp.
Wallace, A.R., 2005. Sedimentation, faulting, and erosion in the Carlin basin, northeastern Nevada, and implications for mineral exploration and ground water resources. In: Rhoden, N.H., Vikre, P.G. (Eds.), Geological Society of Nevada Symposium 2005: Window to the World, Reno, Nevada, May 2005, pp. 147–159.
Wallace, A.R., Perkins, M.E., Fleck, R.J., 2008. Late Cenozoic paleographic evolution of northeastern Nevada: evidence from sedimentary basins. Geosphere 4, 36–74. doi:10.1130/GES00114.1.
Wegmann, K.W., Zurek, B.D., Regalla, C.A., et al., 2007. Position of the Snake River watershed divide as an indicator of geodynamic processes in the greater Yellowstone region, western North America. Geosphere 3, 272–281. doi:10.1130/GES00083.1.
Westaway, R., 1989. Deformation of the NE Basin and Range Province: the response of the lithosphere to the Yellowstone plume? Geophysical Journal International 99, 33–62.
Wolfe, J.A., Schorn, H.E., Forest, C.E., Molnar, Peter, 1997. Paleobotanical evidence for high altitudes in Nevada during the Miocene. Science 276, 1,672–1,675.
Wolff, J.A., Ramos, F.C., Hart, J.D., Patterson, J.D., Brandon, A.D., 2008. Columbia River flood basalts from a centralized crustal magmatic system: Nature Geoscience, published online February 10, 2008. doi:10.1038/ngeo124, 4 pp.
Wood, S.H., Clemens, D.M., 2002. Geologic and tectonic history of the western Snake River Plain, Idaho and Oregon. In: Bonnichsen, Bill, White, C.N., McCurry, Micheal (Eds.), Tectonic and Magmatic Evolution of the Snake River Plain Volcanic Province: Idaho Geologic Survey Bulletin, vol. 30, pp. 69–103.
Wright, T.L., Mangan, M., Swanson, D.A., 1989. Chemical data for flows and feeder dikes of the Yakima Basalt Subgroup, Columbia River Group, Washington, Oregon, and Idaho, and their bearing on a petrological model. U.S. Geological Survey Bulletin 1821. 71 pp.
Xue, M., Allen, R.M., 2006. Origin of the Newberry hotspot track: evidence from shear-wave splitting. Earth and Planetary Science Letters 244, 315–322.
Xue, M., Allen, R.M., 2007. The fate of the Juan de Fuca plate: implications for a Yellowstone plume head. Earth and Planetary Sciences Letters 264, 266–276. doi:10.1016/j.epsl.2007.09.047.
Yuan, H., Dueker, K., 2005. Teleseismic P-wave tomogram of the Yellowstone plume. Geophysical Research Letters 32 (L07304). doi:10.1029/2004GL022056.
Zandt, G., Humphreys, E., 2008. Toroidal mantle flow through the western U.S. slab window. Geology 36, 295–298.
Zoback, M.L., Thompson, G.A., 1978. Basin and Range rifting in northern Nevada: clues from a mid-Miocene rift and its subsequent offsets. Geology 6, 111–116.
Zoback, M.L., McKee, E.H., Blakely, R.J., Thompson, G.A., 1994. The northern Nevada rift: Regional tectono-magmatic relations and middle Miocene stress direction. Geological Society of America Bulletin 106, 371–382.